NUREG-0778

An Assessment of the Failure Rate for the Beltline Region of PWR Pressure Vessels During Normal Operation and Certain Transient Conditions

U.S. Nuclear Regulatory Commission

Office of Nuclear Reactor Regulation

R. M. Gamble, J. Strosnider, Jr.

Available from

GPO Sales Program
Division of Technical Information and Document Control
U. S. Nuclear Regulatory Commission
Washington, D. C. 20555

Printed copy price: $4.50

and

National Technical Information Service
Springfield, Virginia 22161

NUREG-0778

An Assessment of the Failure Rate for the Beltline Region of PWR Pressure Vessels During Normal Operation and Certain Transient Conditions

Manuscript Completed: March 1981
Date Published: June 1981

R. M. Gamble*, J. Strosnider, Jr.

*Presently with EDS Nuclear, Bethesda, MD 20016

Division of Engineering
Office of Nuclear Reactor Regulation
U.S. Nuclear Regulatory Commission
Washington, D.C. 20555

ABSTRACT

A study was conducted to assess the failure rate for the beltline region of a generic pressurized-water reactor (PWR) pressure vessel. This assessment included the evaluation of several normal operating and transient reactor conditions. Failure rates were calculated from a computer code that used fracture mechanics methods to model the failure process; random number generation techniques were used to simulate random variables and model their interaction in the failure process.

This investigation had three major objectives: (1) to better define the effect of neutron irradiation, material variation, and flaw distribution on the failure rate for the beltline region of PWR pressure vessels, (2) to estimate the relative margins against failure for normal operation and certain transient conditions associated with nuclear pressure vessels, and (3) to evaluate the current limitations for using fracture mechanics models to predict failure rates for nuclear pressure vessels.

The calculated results indicate that the failure rates corresponding to operational limits specified by the Boiler and Pressure Vessel Code of the American Society of Mechanical Engineers (ASME Code) and material requirements specified by federal regulation generally provide acceptable safety margins; sensitivity studies completed in the investigation indicate that the failure rates are likely to be accurate within one to somewhat less than two orders of magnitude. The sensitivity studies also define the degree of influence of flaw distribution, material variations, and operating limits on failure rate and provide a means to evaluate the relative levels of reliability associated with different variable values and operating limits.

Blank Page

CONTENTS

CONTENTS (Continued)

FIGURES

FIGURES (Continued)

TABLES

1 INTRODUCTION

Design and fabrication practices for pressure vessels provide a high degree of reliability. This reliability has been demonstrated by the relatively few service failures in nonnuclear pressure vessels and the absence of failures in nuclear pressure vessels. However, because of the significant economic costs and the safety hazards associated with catastrophic pressure-vessel failure, various studies continue to be done so that increasingly accurate estimates for pressure-vessel reliability can be obtained.

Generally, pressure-vessel reliability studies employ either of two methods to calculate the probability of failure and to define reliability. These methods are (1) the analysis of statistical data from observed nonnuclear failures to infer failure rates for both nuclear and nonnuclear pressure vessels and (2) the use of mathematical models that predict failure rates by analytically generating pressure-vessel failures.

Studies completed in Europe and the United States provide estimates of nuclear-pressure-vessel failure rates based on statistical data analyses of past failures. For example, results from European studies (Refs. 1, 2) indicate that the disruptive-failure rate (loss of the pressure-retaining boundary) for nonnuclear pressure vessels is approximately 10^{-5} per vessel year at a 99% confidence level. Various investigations conducted in the United States (Refs. 3, 4) concluded that the disruptive-failure rate at a 99% confidence level is less than 10^{-6} per vessel year for pressure vessels designed, fabricated, inspected, and operated in accordance with the Boiler and Pressure Vessel Nuclear Codes of the American Society of Mechanical Engineers (ASME) (Ref. 5).

Several studies using mathematical models to predict failure rates of nuclear pressure vessels also have been completed in Europe and the United States. In these investigations, the mathematical models contain specific random variables associated with pressure-vessel stresses, temperatures, material characteristics, and the assumed failure process. Because the failure process typically is assumed to result from flaws which are present in the pressure-vessel material, fracture-mechanics relationships usually are the bases for

the mathematical models. The fracture-mechanics relationships include a statistical representation of flaws in the volume of the vessel material and a determination of a critical flaw size that is associated with unstable flaw growth and predicted vessel failure. The statistical flaw distribution in the vessel material volume also often includes an estimate of incremental fatigue crack growth from repetitive stresses during service.

An early study (Ref. 6) that used fracture-mechanics models to predict pressure-vessel failure rates determined that the failure probability for the beltline region of the reactor pressure vessel (the area surrounding the nuclear core) in a pressurized water reactor (PWR) is approximately 10^{-8} per vessel year. However, the mathematical model used in this investigation did not include neutron irradiation.

Later, a comprehensive investigation (Ref. 7) conducted in the United Kingdom determined the failure probability for PWR pressure vessels. The study included (1) a review of nonnuclear pressure-vessel failures, including consideration of design, fabrication, and inspection rules for nuclear vessels, and (2) fracture-mechanics analyses to calculate failure probabilities in various distinct geometric sections of the vessel, including the head, nozzle, and beltline regions. The results of the study, commonly referred to as the Marshall Report, indicated that the head and nozzle regions of the vessel had the highest calculated failure rates for normal and postulated accident conditions, respectively. However, near the end of design life of the vessel, after the pressure-vessel beltline region had accumulated significant neutron irradiation, the failure probabilities for the head, nozzle, and beltline regions of the vessel did not differ significantly. As a result of the investigation, it was concluded that the failure rate for PWR pressure vessels constructed and inspected in accordance with the ASME nuclear codes is less than 10^{-6} per vessel year.

A study to establish additional protective measures in PWRs to reduce the likelihood of pressure-vessel failure from inadvertent pressure transients recently was completed in the United States (Ref. 8). The transient events considered in the study occurred at relatively low temperatures; they were observed when the operating limits established for normal startup and shutdown

of reactor pressure vessels were occasionally exceeded. As part of the evaluation of these transients, a computer code, OCTAVIA (Ref. 9), was constructed to calculate the probability of flaw-induced fracture in the beltline regions of reactor pressure vessels as a result of the transients. To help confirm the necessity to implement additional protective measures for PWRs, OCTAVIA was used to perform several parametric analyses to estimate the probability of failure of the reactor pressure vessels as a function of neutron fluence and the temperature at which the transients typically occurred. The calculated results indicated that if protective measures were not implemented and events were allowed to continue at the previously observed frequency, the failure rate of reactor pressure vessels typically would increase by approximately two orders of magnitude after 10 or more years of plant operation.

Previous studies using fracture-mechanics models to predict failure rates provide substantial information concerning the potential for failure of nuclear reactor pressure vessels. However, areas remain where additional work would permit significant improvement in defining the influence of operational and material variables on the potential for failure of pressure vessels. These areas include (1) the effects of radiation on material resistance to fracture, especially over a wide range of operational temperatures, and (2) the effects of flaw distribution and material variation within a reactor vessel.

Operating experience with PWRs over the past few years has provided additional information that more clearly defines both material variations in reactor pressure vessels and the effect of neutron irradiation on the material resistance to flaw-induced fracture. This additional information establishes improved bases for predicting failure rates for nuclear pressure vessels through the use of fracture-mechanics models. The purpose of this report is to use this recently obtained information with fracture-mechanics models to perform a comprehensive appraisal of the potential for flaw-induced fracture in the beltline region of a generic PWR pressure vessel. This study had three objectives: (1) to better define the effect of neutron irradiation, material variation, and flaw distribution on the failure rate of the beltline region of PWR pressure vessels, (2) to estimate the relative margins against failure for

normal operation and certain transient conditions associated with nuclear reactor pressure vessels, and (3) to evaluate the current limitations for using fracture-mechanics models to predict precise failure rates for nuclear pressure vessels.

The scope of this study is described in Chapter 2. The methods used to calculate failure rates of reactor vessels are contained in Chapter 3. Chapter 4 presents a description of the variables that create the potential for and provide resistance to flaw-induced fracture in nuclear pressure vessels. The results and discussion of the results from this study are presented in Chapters 5 and 6, respectively.

2 SCOPE OF STUDY

During this study, estimates for the probability of flaw-induced fracture in the beltline region of a generic reactor pressure vessel in a PWR were obtained as a function of neutron fluence. These estimates included the evaluation of specific pressure and temperature conditions associated with both normal operation and certain transient events that have occurred or that are postulated to occur in PWRs. In all, five operational events were evaluated for a variety of material conditions in the vessel beltline. Sections 2.1 and 2.2 describe the operational events and the beltline geometry and material conditions included in the study, respectively.

2.1 Operational Events

2.1.1 Normal Operation

For normal operation, pressure and temperature conditions corresponding to startup, shutdown, and full-power operation were evaluated. Normal startup and shutdown of nuclear reactor pressure vessels take place in the so-called material-transition-temperature region, where the material resistance to flaw-induced fracture significantly changes with and is directly proportional to material temperature. Because there is a significant change in the fracture resistance of material in the transition-temperature region, reactor startup and shutdown operations are carefully controlled, and they proceed along specific pressure/temperature paths that are established to protect the reactor vessel against flaw-induced fracture. These pressure/temperature paths define the maximum normal operating pressure that should be applied to the vessel at any specified temperature; they are constructed using procedures contained in the ASME Boiler and Pressure Vessel Code (Ref. 10). Because neutron irradiation diminishes the fracture resistance of nuclear-pressure-vessel steels at any temperature in the transition region, the allowable pressure-temperature paths change with neutron irradiation. To determine the potential for flaw-induced fracture during normal startup and shutdown operation, failure rates were calculated for various individual pressure/temperature combinations in the transition-temperature region at specific neutron-fluence levels. The results of these calculations were used to define

distinct, continuous pressure/ temperature paths that correspond to startup and shutdown operation at constant failure rates and specific neutron fluence levels. To illustrate the relative margins against flaw-induced fracture that are provided by ASME code procedures, the pressure/temperature paths established by the failure-rate calculations were compared to the paths specified by the code.

As reactor startup operations proceed through the transition temperature region toward higher temperatures, the resistance to flaw-induced fracture of the metal in the reactor pressure vessel increases until it reaches a plateau and, ideally, remains constant with increased temperature. This plateau is called the upper-shelf fracture toughness, and the temperature range where the plateau is maintained is the upper-shelf temperature region. Normal full-power operation of PWR reactor pressure vessels at 2250 psi and 550°F typically takes place in the upper-shelf temperature region.

In the upper-shelf temperature region, the fracture resistance of irradiated pressure-vessel steels can be expressed as a function of the initial unirradiated upper-shelf fracture toughness and a decrease in the initial value as a result of neutron irradiation. To determine the potential for flaw-induced fracture during normal full-power operation, failure rates were calculated as a function of unirradiated and irradiated upper-shelf fracture toughness. The results from these calculations were used to illustrate the relative margins against flaw-induced fracture provided by requirements for material upper-shelf fracture resistance that are contained in Title 10 of the Code of Federal Regulations Part 50 (10 CFR 50) (Ref. 11). These requirements are twofold: (1) the unirradiated upper-shelf fracture toughness stated in terms of Charpy V-Notch (CVN) absorbed energy must be at least 75 ft-lb, and (2) the irradiated upper-shelf CVN energy must remain above 50 ft-lb.

2.1.2 Transient Events

In addition to normal operating conditions, two transient events were evaluated. These transients were (1) the inadvertent pressure transients (previously discussed) that periodically exceeded the ASME Code pressure/ temperature limits established for normal startup and shutdown of the reactor

pressure vessel in the transition-temperature region (Ref. 8) and (2) pressure transients that are postulated to occur in the upper-shelf temperature region during full-power operation. For the transients that had occurred in the transition-temperature region, calculations of failure rate were performed using the event frequency observed before the implementation of protective measures, as well as statistical representations for the pressure and temperature spectra over which the transients occurred.

The probability of flaw-induced fracture associated with postulated pressure transients in the upper-shelf temperature region was calculated at 550°F for several postulated pressure levels above the normal operating pressure of 2250 psi. The probabilities that the events actually would occur and that the postulated pressure levels would be reached were not determined in this study.

2.2 Vessel Beltline Characteristics

The beltline regions of reactor pressure vessels in PWRs designed in the United States have a range of sizes, fabrication configurations, neutron-irradiation levels, and material characteristics. To determine the potential for flaw-induced fracture in the beltline region of a generic reactor pressure vessel in a PWR, average beltline dimensions, two typical fabrication configurations, and two neutron-irradiation levels were chosen for analysis; the material characteristics generally were treated as random variables. The vessel geometry and material variables are representative of PWRs currently operating in the United States. However, the material random variables also were included in several sensitivity analyses that enable the results obtained for typical operating PWRs to be extended to PWRs that are now either under construction or planned for construction.

2.2.1 Beltline Geometry and Flaw Distribution

When failure rates are predicted using fracture mechanics models, flaw size generally is given a statistical representation associated with a specified material volume. In this investigation, the material volume used to establish the flaw distributions is based on the volume of weld metal in the beltline of the pressure vessel rather than on the total material volume in the beltline.

Only the weld volume is used because, compared to the base metal, it is more likely to contain cracks or defects, and it generally is more sensitive to neutron irradiation, as indicated by test results from surveillance programs at operating PWRs.

The weld volume and orientation in the beltline region of a reactor pressure vessel vary depending on whether the beltline shell is fabricated from rolled plates or forged rings. Figure 2.1 illustrates two beltline weld configurations (Ref. 7); the shaded areas in Figures 2.1a and 2.1b indicate the weld volumes and orientations used in this study for beltline shells fabricated from rolled plates and forged rings, respectively.

The analyses in this investigation included consideration of fatigue crack growth from repetitive loading during service; however, specific flaw-growth calculations were not performed. Instead, failure rates were calculated using the preservice, and end-of-design-life flaw distributions contained in the Marshall Report, as well as the end-of-design-life distribution contained in the OCTAVIA code. The evaluation of these distinct distributions provided an estimate of the maximum relative effect of fatigue-flaw growth on failure probability and indicated the sensitivity of calculated failure probability to a range of assumed flaw distributions. The analyses did not include consideration of inservice inspections that may be performed periodically during service to detect flaws in the pressure-vessel welds.

2.2.2 Beltline-Material Variables

The resistance to flaw-induced fracture of irradiated pressure vessels is a function of several variables, including metal temperature, material residual-element content, and neutron fluence.

Neutron fluence is a function of time at operation and the distance between the material and the neutron source. In this study, failure rate calculations were performed at two neutron-fluence levels corresponding to 10 effective full-power years (EFPY) of operation and end-of-design-life (EOL) operation.

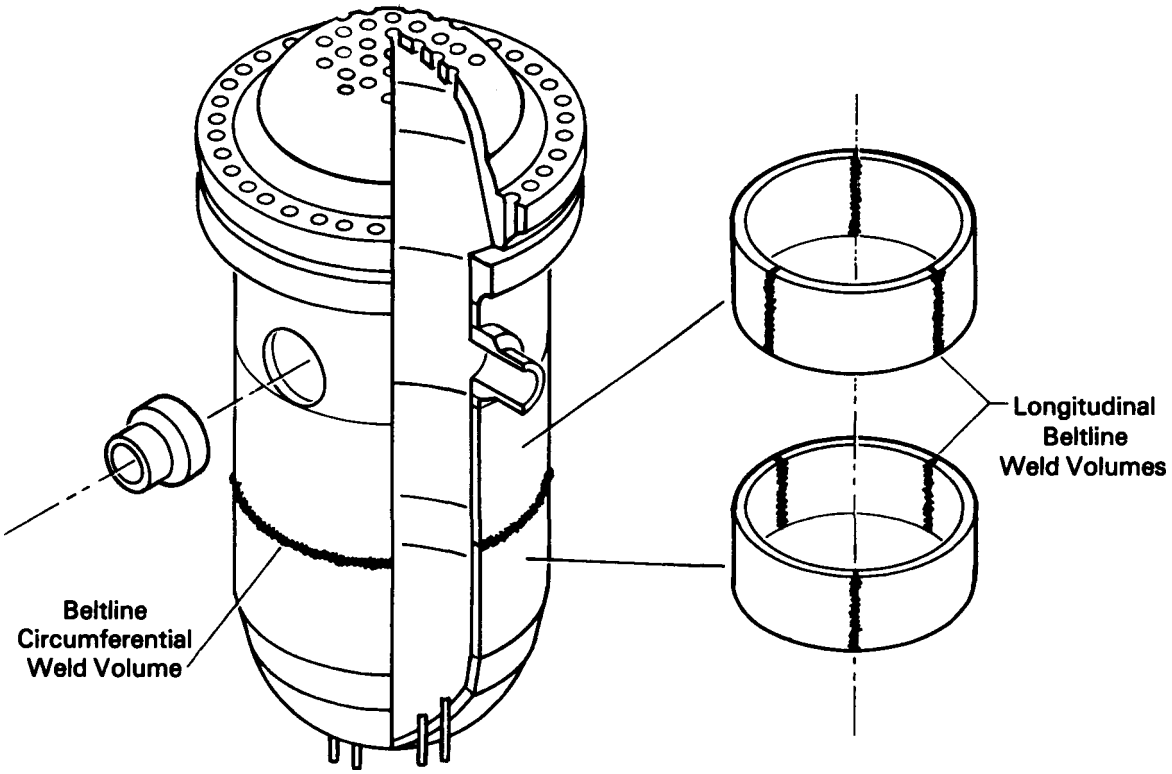

1(a) Rolled and Welded Beltline Shell

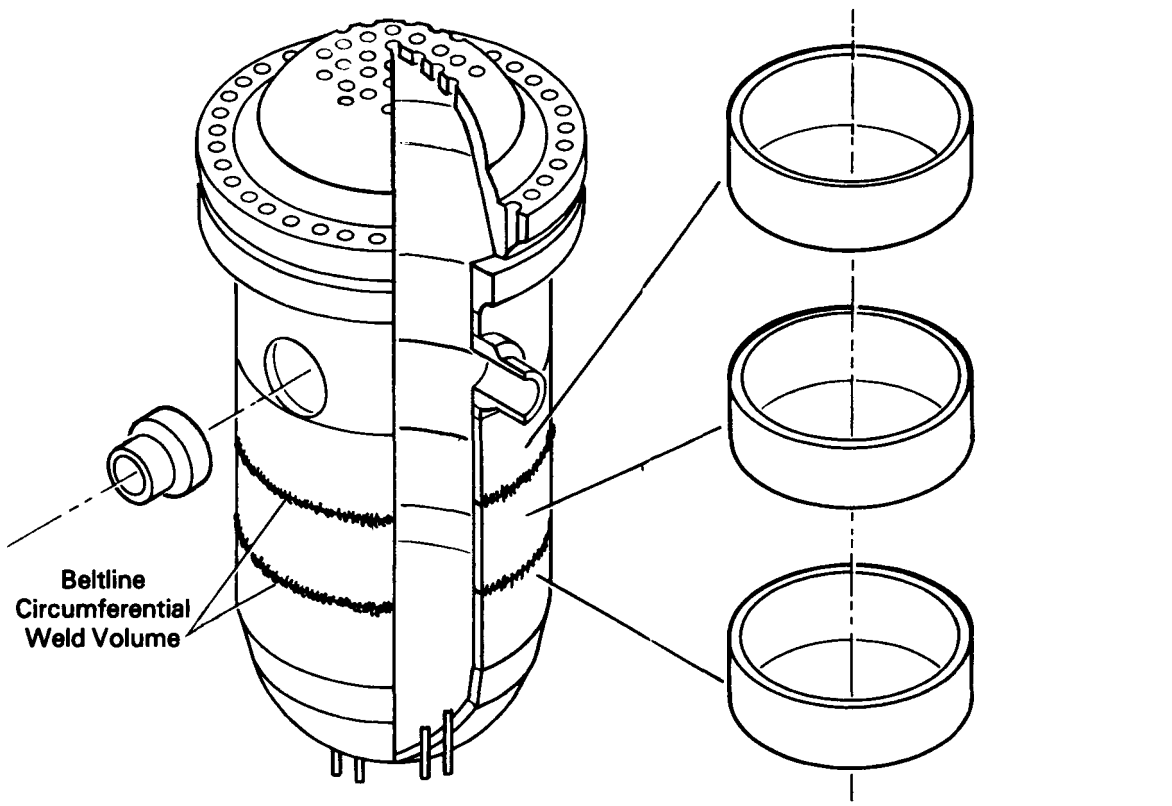

1(b) Welded-Ring-Forging Beltline Shell

Figure 2.1: PWR Beltline Shell Fabrication Configurations

Several residual elements either enhance or degrade material fracture resistance in irradiated reactor-vessel steels. The residual elements used in this study are copper and phosphorous; both degrade fracture resistance. Only copper and phosphorous are included because the largest amounts of data that describe the effect of residual-element content on fracture resistance of irradiate pressure-vessel steels have been obtained using these elements. Copper is known to have significant variation in the weld volume of operating PWRs; consequently, copper content is used as a random variable throughout this study. An estimate of the distribution of copper content was obtained from data reported for operating PWRs. Although statistical descriptions of copper content are not reported for individual plants, a generic distribution was developed by assuming that the distribution through the weld volume for any one plant was reasonably modeled by the distribution obtained from the combination of single copper values individually reported for single vessels. The accuracy of this assumption cannot be assessed rigorously; however, intuition suggests that this is a realistic approximation, based on fabrication practice and the materials used in the fabrication of most operating PWRs. Although phosphorous--like copper--is a random variable, a single, constant value was used for all failure-rate calculations. Use of a single, constant value was dictated by the lack of data for phosphorous content.

Several parametric studies also were conducted to determine the effect of copper content on failure rate. These studies included distributions estimated to be representative of newer reactor vessels with lower and less-variable copper content and of single values of copper content corresponding to those typically used to construct the ASME code pressure/temperature limits.

Because significant variations in material-fracture resistance may occur for any given set of material conditions, fracture resistance also is used as a random variable throughout this study. A description of a distribution for fracture resistance was estimated using data from several heats of irradiated and unirradiated reactor-vessel steels. Although these data are believed to provide a realistic estimate of the mean fracture resistance, they are considered insufficient to define the type and dispersion of the distribution; these were estimated. The dispersion was included in a parametric study to determine the effect of the range of fracture resistance on calculated failure rate.

3 METHODOLOGY

A computer code was developed to calculate the probability of flaw-induced failure in the beltline region of irradiated PWR reactor pressure vessels. The computer code uses mathematical relationships based on linear elastic fracture mechanics to model variable interaction and estimate failure rate. The failure criterion contained in the model is based on a comparison of the potential for flaw-induced fracture, K_I, with the material resistance to flaw-induced fracture, K_{IC}. Reactor-vessel failure is predicted when $K_I \geq K_{IC}$.

Values of K_I and K_{IC} are determined by combinations of operational and material variables. In general terms, the potential for flaw-induced fracture, K_I, depends on the flaw size, a, and stress, σ, in the pressure vessel. The resistance to flaw-induced fracture, K_{IC}, is a function of the temperature of the metal of the vessel, T; neutron fluence; and copper and phosphorous contents.

For convenience, neutron fluence and copper and phosphorous content are usually combined into an equivalent temperature parameter, RT_{NDT}, called adjusted reference temperature. The parameter RT_{NDT} represents a measure of the initial unirradiated material fracture resistance and a change in this resistance as a result of neutron irradiation. When combined, the metal temperature and the adjusted reference temperature allow the fracture resistance, K_{IC}, to be described as a function of temperature alone.

Because many of these variables are random variables with complex interactions, the computer code uses Monte Carlo methods of random number generation (Refs. 12, 13) to simulate independently each of several random variables from their respective statistical distributions, and it combines these variables to obtain K_I and K_{IC}. Figure 3.1 illustrates the computer-simulation cycle used to simulate the random variables, model their interaction to obtain K_I and K_{IC}, and predict failure in reactor vessels. The variables that typically are considered random variables in this study are designated "simulate" in Figure 3.1.

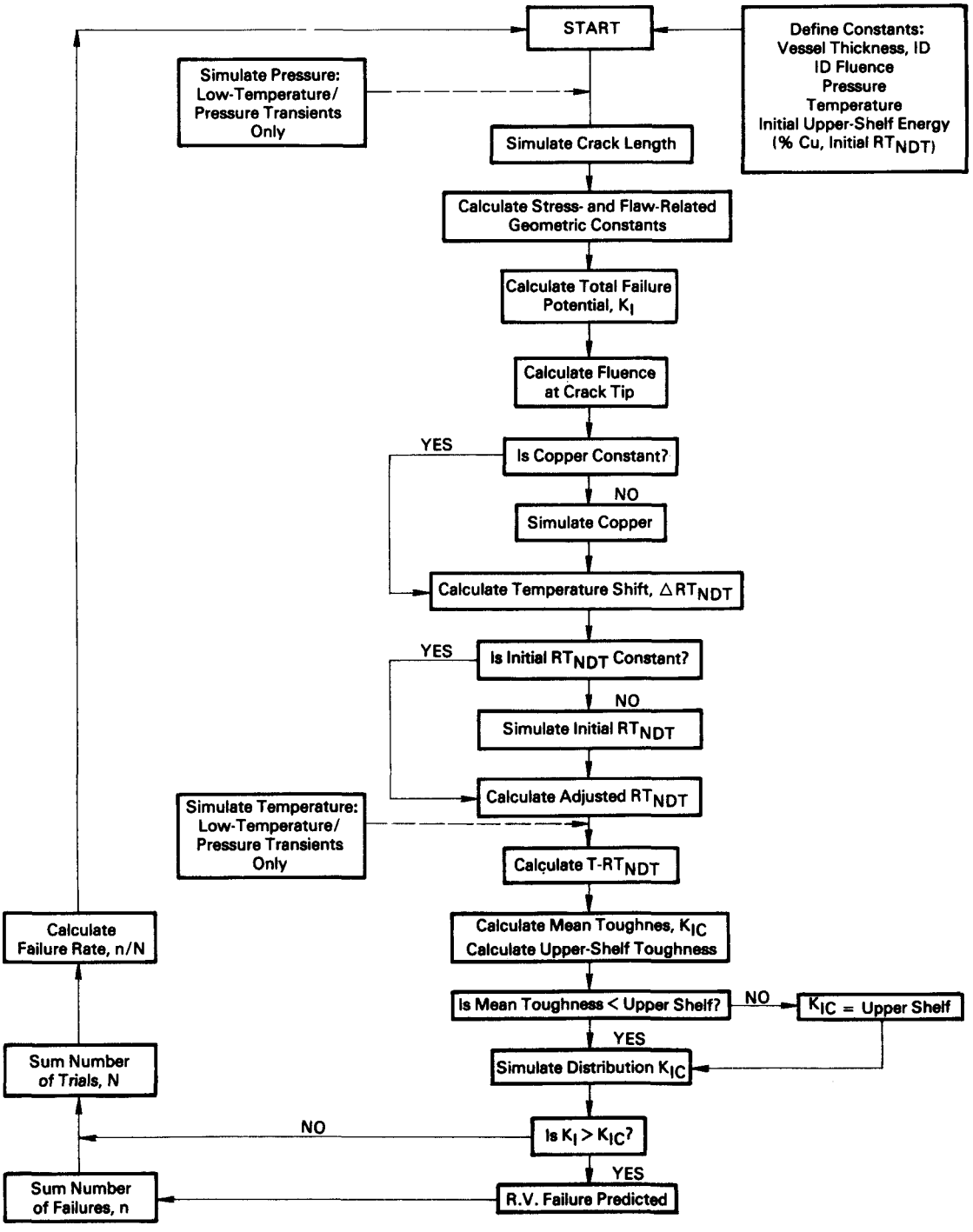

FIGURE 3.1: Representation of Simulation-Failure Model

The simulation cycle depicted in Figure 3.1 represents a single computer experiment conducted to determine if a single occurrence of a specific operational event will produce failure of the reactor vessel. To estimate the failure rate associated with that specific operational event, the cycle is repeated up to 10 million times, and new values of the random variables are generated each time. The failure rate is then estimated from the ratio of the number of observed experimental failures to the total number of experimental trials. The failure rate calculated by the computer code gives the unit failures per event; mutiplying this result by the anticipated number of events per vessel year will give the more commonly used unit failures per vessel year.

Because the computer code required to model the simulation cycle in Figure 3.1 is relatively large and complex, several checks were made during the development of the code to ensure that accurate results are obtained. First, failure probabilities associated with the previously described low-temperature/pressure transients (Ref. 8) were calculated and these probabilities were compared to the results obtained from the closed-form solutions in the OCTAVIA code (Ref. 9). This comparison indicated relatively good agreement; the detailed results of the comparison are presented in Appendix A to this report. Additionally, computations were made over a wide range of operational conditions and associated failure probabilities to obtain a practical estimate of the number of simulated failures that would provide adequate results. These computations indicated that approximately 10 simulated failures were sufficient to provide results that were within a factor of 3 of the steady-state result obtained from several hundred simulated failures.

Near the end of this study, an importance-sampling scheme was developed and incorporated into the computer code to increase the code's efficiency for performing calculations in the transition-temperature region. This scheme also allowed more precise accuracy checks to be made at a specified confidence level and was particularly useful for analyzing conditions associated with low-failure probabilities. A description of the importance-sampling scheme is presented in Appendix B to this report.

4 DEFINITION OF VARIABLES

4.1 Generic Beltline Geometry

In this investigation, the beltline geometry for a generic pressure vessel in a PWR has an 8-in. wall thickness and an 80-in. mean radius. The average end-of-design life (EOL) neutron fluence at the inner surface generic beltline shell is 4×10^{19} neutrons per square centimeter (n/cm^2).

4.2 Potential for Flaw-Induced Fracture

The potential for flaw-induced fracture, K_I, is a function of the applied stress, the stress distribution, and the crack size, shape, and location in the vessel. In general, the calculated potential for flaw-induced fracture includes individual components for pressure, thermal, and residual stress and has the form

$$K_I = \alpha\sqrt{\pi a} \sum_{i=1}^{3} \sigma_i F_i \qquad (1)$$

where a = radial depth of a flaw that extends from the vessel surface part way through the vessel wall

α = flaw shape factor

σ_i = maximum stress for the i^{th} stress distribution

F_i = modifying function for the i^{th} stress distribution

The F_i functions for the pressure, thermal, and residual stress distributions are shown in Figure 4.1 as functions of the ratio of the surface flaw depth, a, to the vessel wall thickness, t. The pressure stress used in equation (1) is obtained from membrane theory. A residual-stress distribution for beltline welds was estimated to be sinusoidal, with maximum tensile stress of 8 kips per square inch (ksi) at the inner and outer surfaces of the vessel wall and compression at the midwall of the vessel. Thermal stresses were used only for startup and shutdown operations and were estimated by a pure bending distribution, with a maximum surface stress of 4 ksi. The magnitude of the thermal stress distribution corresponds to a heatup or cooldown rate of 50°F per hour. The value of the flaw shape factor, α, in this study is constant and is equal to

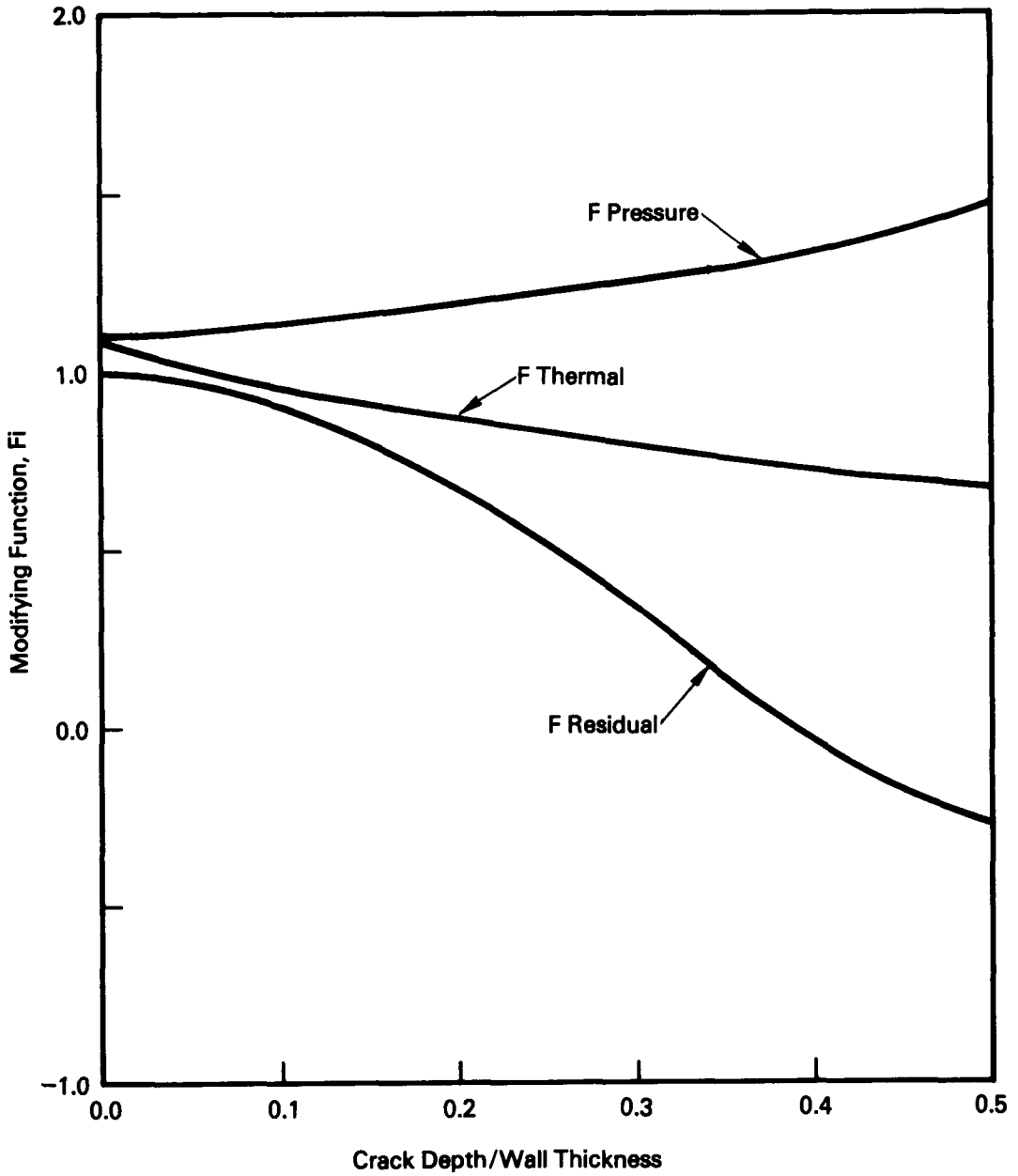

Figure 4.1: Stress-Intensity-Modifying Function vs a/t

0.89; this value corresponds to a semi-elliptical, finite length surface flaw with a depth-to-length ratio of 1 to 6.

The independent variables used to determine K_I for each simulation cycle are pressure and crack depth, a. Except during the analyses of low-temperature/pressure transients, the operational pressure is held constant for the total number of experimental computer trials, and it corresponds to a specific operational event for which the failure probability is being calculated. During each of the individual simulation cycles, the random variable crack depth is simulated from a statistical distribution representative of the volumes and orientations of the welds in the beltline of the reactor vessels (previously illustrated in Figure 2.1). The residual and thermal stresses are a function of crack depth and are calculated during each simulation cycle at the simulated crack length. The thermal stress is included only during the analyses of normal startup and shutdown conditions. During the remaining operational events, the thermal stress is assumed equal to zero.

Although the data obtained from operating PWRs provide adequate bases for defining most of the variables needed to complete this study, very little data are available to describe accurately the number and size of the flaws in the material volume of a reactor pressure vessel. The flaw distribution is, of course, difficult to define quantitatively since the flaws of interest are not the flaws that have been detected but those of unknown size and number that remain in the vessel material because they were not detected. Because of this difficulty, no attempt was made in this study to gather data to construct precise flaw distributions. Instead, the distributions contained in the Marshall Report (Ref. 7) and the OCTAVIA code (Ref. 9) were used. There are no known new data to indicate that these two previously developed distributions should be modified for this investigation.

The flaw distributions obtained from the Marshall Report and the OCTAVIA code are shown in Figure 4.2 for the various weld volumes and orientations in PWR beltlines. The dashed lines are the distributions developed from the Marshall Report, and the solid line corresponds to the OCTAVIA distribution. The weld volume associated with the OCTAVIA flaw distribution was defined (in Ref. 9) generally as the volume of longitudinal weld in the beltline region of a PWR

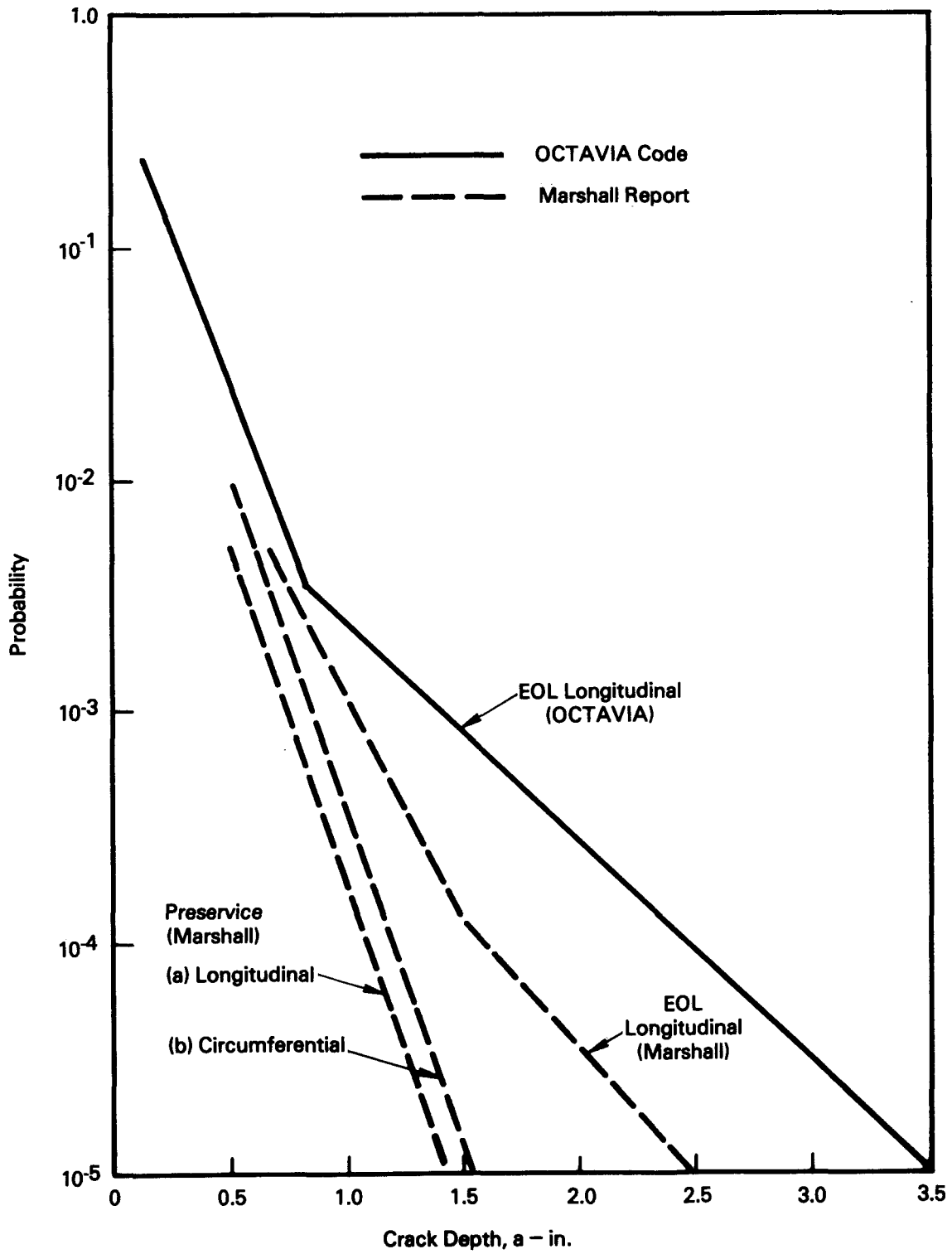

Figure 4.2: Reactor-Vessel-Beltline Flaw Distributions

without specific reference to the total vessel volume. The Marshall Report defined the flaw distribution in terms of the total volume of the reactor vessel. To obtain flaw distributions for the beltline welds considered in this study, the longitudinal beltline weld volume illustrated in Figure 2.1(a) was estimated as one hundredth of the total vessel volume; the circumferential beltline weld volume illustrated in Figure 2.1(b) was estimated as one fiftieth of the total vessel volume.

The dashed line on the far left in Figure 4.2 represents the preservice crack distribution for the volume of longitudinal beltline weld. The second dashed line from the left represents the preservice crack distribution for the volume of circumferential beltline weld. The dashed curve on the right and the solid curve are from the Marshall Report and OCTAVIA code, respectively; they represent the end-of-life crack distributions, including fatigue crack growth in water environment, for the volume of longitudinal beltline weld.

In all instances, the flaw distributions represent semi-elliptical surface cracks whose major axes are oriented parallel to the weld direction. It is assumed that there is no interaction between individual cracks in the weld volume.

For illustration, the crack depth, a, in Figure 4.2 is represented as a continuous random variable. However, in this study, as well as in the OCTAVIA code, the crack depth is used as a discrete random variable. For each curve in Figure 4.2, approximately nine distinct crack depths ranging from 0.25 to 3.5 in. and the probabilities indicated at these crack depths were used to construct stepwise cummulative probability distributions. The Monte Carlo simulation in the computer code used the stepwise cummulative distributions to generate a crack depth for each simulation cycle. A discrete random variable is used because (1) there are insufficient data from which to infer a continuous statistical distribution, (2) the computer code calculational procedure provides a computational efficiency when it is used with a discrete random variable, and (3) it provides a viable way to estimate the effect of minimum detectable flaw sizes as discussed in Chapter 5.

4.3 Resistance to Flaw-Induced Fracture

4.3.1 Fracture-Toughness Representation

4.3.1.1 Transition-Temperature Region

Figure 4.3 presents experimental data and an associated estimated mean curve that represent the material resistance of reactor vessel to flaw-induced fracture, K_{IC}, in the transition-temperature region. The material resistance to flaw-induced fracture, or fracture toughness, is presented as a function of the independent variable ($T-RT_{NDT}$), where the material temperature, T, is indexed by the adjusted reference temperature, RT_{NDT}. Indexing the material temperature by RT_{NDT} is commonly used to generalize the fracture-toughness/temperature relationship by accounting for service-induced material changes and variation in initial material-toughness properties.

The index temperature, RT_{NDT}, is the sum of an initial, unirradiated value of RT_{NDT} and a change (increase) in this initial value as a result of neutron irradiation. The initial RT_{NDT} is regarded as a material property and is defined by the ASME code (Ref. 14). The increase in RT_{NDT} for the weld metal during neutron irradiation is enhanced by increased material copper and phosphorus contents and is calculated by the computer code from previously developed empirical relationships (Ref. 15). As indicated in Figure 4.3, the increase in RT_{NDT} is the variable that directly relates loss of fracture toughness to neutron irradiation at any specified material temperature.

The experimental data in Figure 4.3 include base and weld metals in both the irradiated and unirradiated conditions. The unirradiated data are test results from the heavy section steel technology (HSST) program (Ref. 16) and from several surveillance programs from operating PWRs. The irradiated data are from surveillance programs of operating reactors only. The data were obtained from either compact-tension or wedge-opening-loading fracture-mechanics specimens; they include only the experimental points where the specimen thicknesses satisfy the ASTM E399 (Ref. 17) size criterion, thickness $\geq 2.5\ (K_{IC}/\sigma_y)^2$.

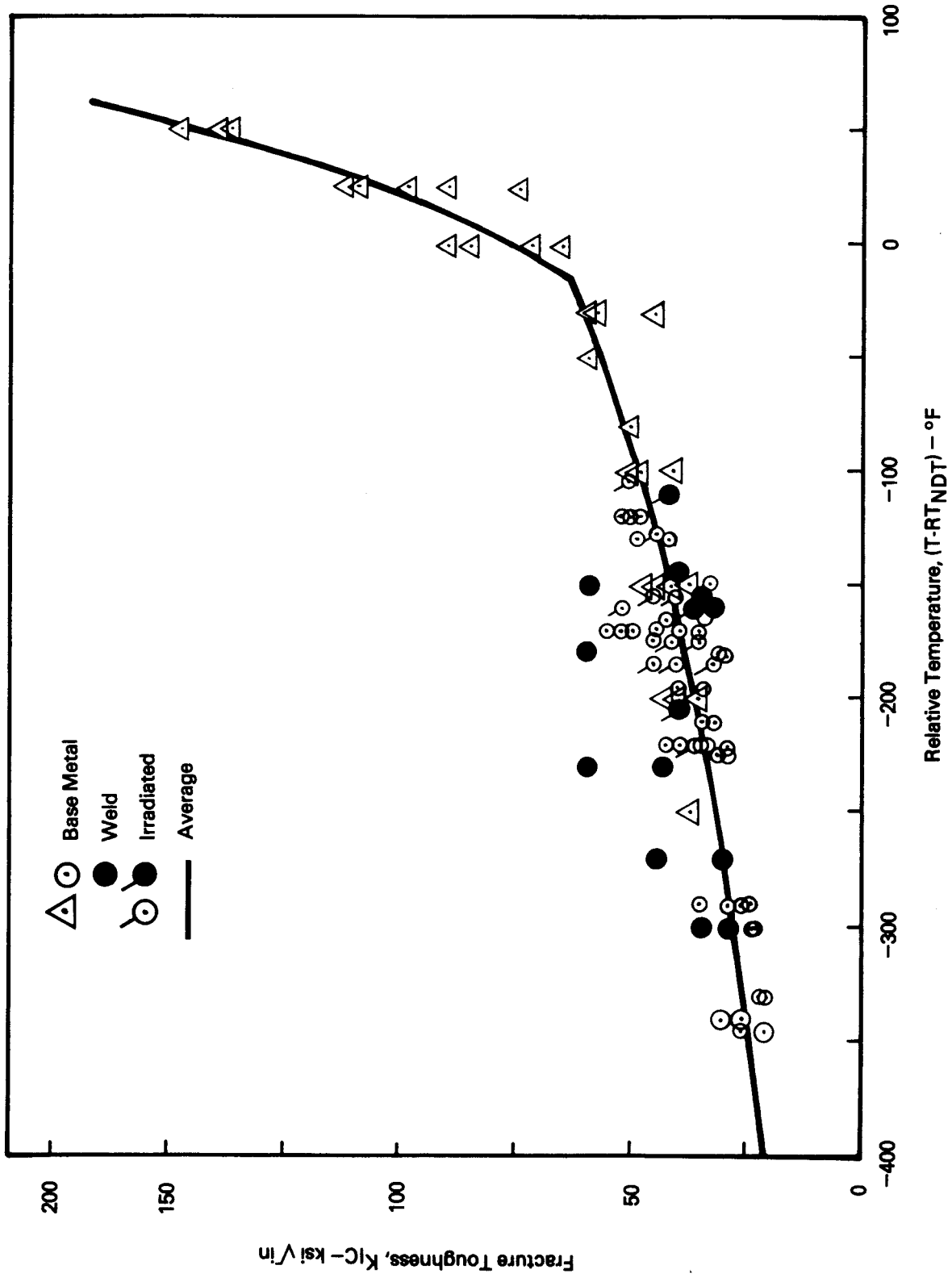

Figure 4.3: Fracture Toughness of Reactor-Vessel Steel vs Relative Temperature

The estimated mean fracture-toughness curve shown in Figure 4.3 is divided into two distinct regions for computational purposes

$$K_{IC} = 10 + 58.0\ e^{[0.004(T-RT_{NDT})]} \qquad (2a)$$

where $-400°F \leq (T-RT_{NDT}) \leq -16°F$, and

$$K_{IC} = 21 + 53.8\ e^{[0.0165(T-RT_{NDT})]} \qquad (2b)$$

where $-16°F < (T-RT_{NDT})$, and $K_{IC} \leq$ upper-shelf fracture toughness

4.3.1.2 Upper-Shelf Temperature Region

As described earlier, the fracture toughness of reactor vessel steels increases with increasing temperature until a plateau called upper-shelf fracture toughness is reached. Because of certain material and test limitations, the upper-shelf fracture toughness generally cannot be measured directly using conventional (Ref. 17) practice. This is a relatively common difficulty for tough materials, and various empirical methods have been developed previously to infer K_{IC} from the more practical Charpy V-Notch test. In this investigation, the mean upper-shelf fracture toughness is estimated from an empirical correlation developed previously by Barsom and Rolfe (Ref. 18), namely,

$$K_{IC} = \sigma_y[5CVN/\sigma_y - 0.25]^{\frac{1}{2}} \qquad (3)$$

where CVN = Charpy V-notch upper-shelf energy, ft-lbs

σ_y = material yield strength, ksi

The independent variable, CVN, decreases with neutron irradiation; this decrease is enhanced by residual element content, especially copper and phosphorus. The computer code uses previously developed empirical

relationships (Ref. 15) to calculate the reductions in CVN for the weld metal as a function of neutron irradiation and copper and phosphorus content. The material yield strength also is a function of neutron irradiation, and it increases with increasing neutron fluence. Throughout this study, however, the irradiated yield strength used in equation (3) is assumed constant over the fluence range considered and is equal to 90 ksi. The magnitude of the mean fracture toughness calculated from equation (3) is limited to a maximum of 220 ksi $\sqrt{in}$.

4.3.1.3 Statistical Distribution for K_{IC}

Because K_{IC} is a random variable, representations of statistical distributions about the mean fracture-toughness values calculated from equations (2) and (3) are necessary to perform the simulation cycle illustrated in Figure 3.1. Since there are not enough data available to rigorously determine a statistical distribution, a normal distribution with a standard deviation, σ, equal to 10 percent of the calculated mean fracture toughness, $\bar{K}_{IC}$, was used in both the upper-shelf and transition-temperature regions (Ref. 7). Stated in operational terms, this assumption means that there is 1 chance in 100 that the actual material fracture toughness, K_{IC}, at any $(T - RT_{NDT})$ will fall outside the range $\bar{K}_{IC} \pm .25\ \bar{K}_{IC}$. Because the fracture-toughness distribution is an estimate, several sensitivity studies were conducted to determine how variations in fracture-toughness limits established by this distribution would affect the calculated failure probability. These studies included varying the allowable simulated toughness limits between the following ranges:

$$\bar{K}_{IC};\ (\bar{K}_{IC} \pm 1\sigma);\ (\bar{K}_{IC} \pm 2\sigma);\ (\bar{K}_{IC} \pm 3\sigma);\ \text{and}\ o < K_{IC} < (\bar{K}_{IC} + 3\sigma)$$

4.3.2 Fracture-Toughness-Related Independent Variables

4.3.2.1 Neutron Fluence

The neutron fluence in the wall of the reactor pressure vessel decreases with distance from inside surface of the vessel. The fluence in the vessel wall at any distance from the inside surface is determined from the relationship

$$f_x = f_I \, e^{-\frac{1}{3}x} \qquad (4)$$

where x = radial distance into the vessel wall from the inside surface

f_I = neutron fluence at the inside surface of the vessel wall

f_x = neutron fluence at position x in the vessel wall

Because K_{IC} is an inverse function of neutron fluence, the value of K_{IC} increases through the vessel wall relative to the inside surface. The values of K_{IC} obtained from equations (2) and (3) are determined using the fluence calculated from equation (4), where the radial distance x corresponds to the location of the tip of the crack relative to the inside vessel surface.

4.3.2.2 Temperature and Adjusted Reference Temperature

As equations (2) and (3) indicate, the calculated mean fracture toughness in the transition and upper-shelf temperature regions is a function of the respective independent variables ($T - RT_{NDT}$) and CVN. In addition to K_{IC} having a statistical distribution at any specified value of these variables, the independent variables also can be random variables.

Generally, the material temperature, T, corresponds to a specific operational condition for which the failure probability is being calculated; it does not vary during the total number of simulation cycles associated with that event. However, as discussed in Chapter 5, T is a random variable during the analyses of low-temperature/pressure transients.

The intial RT_{NDT} is a random variable because significant variations in initial RT_{NDT} are observed for different base and weld metals used in reactor pressure vessels. The changes in RT_{NDT} and CVN which result from neutron fluence are used as random variables in the computer code, primarily because of their dependence on copper content, which can vary significantly through the weld volume. In this study, neutron fluence and phosphorus content are not used as random variables. Fluence is established as a time parameter at

which specific operational events occur. Phosphorus content, like copper content, is a random variable; however, because of the lack of any reliable data, phosphorus content was assumed to be a constant 0.015 percent.

To simulate ($T - RT_{NDT}$) and CVN during the computer experiment, statistical distributions were established for the random variables initial RT_{NDT} and copper content by using data from operating PWRs (Ref. 8). Using these data and statistical significance tests, it was determined that both distributions can be considered normal. The distribution for initial RT_{NDT} has a 23°F mean value and a 20°F standard deviation. The copper content distribution has a 0.23 percent mean and a 0.07 percent standard deviation.

Although these distributions are likely to be good generic representations for copper content and intial RT_{NDT} through PWR weld volumes, some limitations and uncertainties are associated with them. For example, newer PWRs generally have beltline welds with reduced and less-variable copper contents. Additionally, there is an uncertainty associated with the distribution for initial RT_{NDT} because the values obtained for the operating PWRs often were not determined from present code procedures (Ref. 14) but are estimates based on various empirical correlations or experience. To determine how the calculated failure probabilities are affected by the expected variations and uncertainties associated with these distributions, sensitivity studies were conducted over a wide range of simulated and constant values of copper contents and associated values of adjusted reference temperature, RT_{NDT}.

4.4 Reference-Variable Condition

Throughout this study, the failure-rate calculations were performed primarily for a reference group of variables that are thought to be representative of those in operating PWRs. These variables were emphasized because of the immediate interest in operating reactors and because, in many instances, data from operating reactors are better defined. The following variable conditions constitute the reference variable condition in this study:

(1) the OCTAVIA flaw distribution shown in Figure 4.2

(2) a minimum detectable flaw depth, a, of .25 in.

(3) the normal distribution for K_{IC} (described in Section 4.3.1), where K_{IC} is restricted to the region between $\bar{K}_{IC} \pm 3\sigma$

(4) the normal distribution (described in Section 4.3.2) for initial RT_{NDT}

(5) the normal distribution for copper content for operating PWRs (described in Section 4.3.2).

(6) an initial upper-shelf Charpy energy of 65 ft-lbs

(7) flaws located at the inner surface of the vessel

(8) only longitudinal welds at the beltline

The values listed for the first six variables were selected because they best represent realistic material conditions in pressure vessels at many operating facilities. The conditions listed for the last two variables, flaw location and orientation, typically were used throughout the analyses because they are dominant and establish the failure probabilities for the operational events. As shown in Chapter 5, more precise models for flaw location and orientation do not significantly alter the calculated results.

The reference variables were included in various parametric studies. The most extensive parametric studies were conducted for the normal startup and shutdown operational events. The variables in the parametric study for the startup/shutdown events are flaw orientation, flaw location, flaw distribution, minimum detectable flaw size, copper content, K_{IC} range, and neutron fluence.

Parametric studies also were completed for normal full-power operation, anticipated low-temperature/pressure transients, and postulated

high-temperature/pressure transients. Included in the parametric studies for each of these operational events are flaw distribution, minimum detectable flaw size, and neutron fluence. Also included in sensitivity studies are the variables copper content and thermal stress for normal full-power operation and pressure level for the postulated high-temperature/pressure transient.

5 RESULTS

In this chapter, results are presented of analyses which were conducted to calculate failure probabilities of reactor pressure vessels for the five operational events described in Section 2.1. Included are the results of calculations using the reference variable conditions defined in Section 4.4, as well as the results from extensive parametric studies. The results from the parametric studies are especially important because they provide data for a wide range of vessel conditions, identify the most influential variables and variable interactions, and help define limitations to using fracture-mechanics models to predict the failure probability of pressure vessels.

Except for the anticipated low-temperature/pressure transient analyses, the results in the following sections are presented as "the number of failures per operational event." This unit was chosen so that the results could be applied generally for different event frequencies. The results for the anticipated low-temperature/pressure transient analyses are presented as "the number of failures per vessel year." This unit is used to simplify comparisons with results that are available from the OCTAVIA code.

5.1 Normal Startup and Shutdown Operations

This section presents the calculated failure rates obtained for the reference variable condition and various parametric conditions associated with normal startup and shutdown operations of the generic reactor vessel in the transition-temperature region. The calculated results are generally presented as pressure/temperature paths that represent shutdown operation at constant failure rates. The results typically are presented for shutdown operation only because, as one of the parametric studies will show, the shutdown condition is the dominant contributor to failure probability in the startup/shutdown sequence.

5.1.1 Reference Variable Condition

The calculated constant failure-rate pressure/temperature paths for the reference variable condition defined in Section 4.4 are presented in

Figures 5.1 and 5.2 at neutron-fluence levels corresponding to 10 effective full-power years (EFPY) and end-of-design-life (EOL), respectively. Figures 5.1 and 5.2 also contain, for comparison, the pressure/temperature-limit curves established for reactor shutdown by the ASME code.

The comparisons of the code pressure/temperature-limit curves with the calculated failure-rate paths in Figures 5.1 and 5.2 illustrate the calculated relative margins against failure provided by the code limits. Several observations can be made concerning this comparison. First, code-limit curves are constructed using deterministic values for flaw size, flaw orientation, pressure, copper content, and initial RT_{NDT}. Except for copper content and initial RT_{NDT}, each deterministic value is either a conservative bound or is modified by a safety factor. Thus, the comparison between the code limits and the constant failure-rate paths provides a correlation between failure probability and a combination of deterministic safety factors and bounding values.

However, this correlation is not exact, and it depends on the reliability or applicability of the data used to construct the code limit and constant failure-rate curves. For example, in the code procedure, copper content and initial RT_{NDT} are assumed to be well-defined, single values. In reality, copper content varies through the weld volume, and it is difficult to choose the single value that will properly model the effect of copper content. The code-limit curves in Figures 5.1 and 5.2 are constructed using a copper content and initial RT_{NDT} of 0.23% and 23°F, respectively; these numbers correspond to the mean values of the reference distributions used to generate the constant failure-rate paths. For consistency, the 0.23% copper content and the 23°F initial RT_{NDT} are used throughout this report when it is necessary to define single values for these two parameters. By choosing different constant copper contents over a reasonable range of expected values, the position of the code-limit curve and the correlation with the constant failure-rate paths will be changed significantly.

The calculated failure rates and the correlation with code limits are similarly affected by other constant variable values or variable distributions. The results from the parametric studies in the following sections can be used to judge the influence of several variables on calculated failure

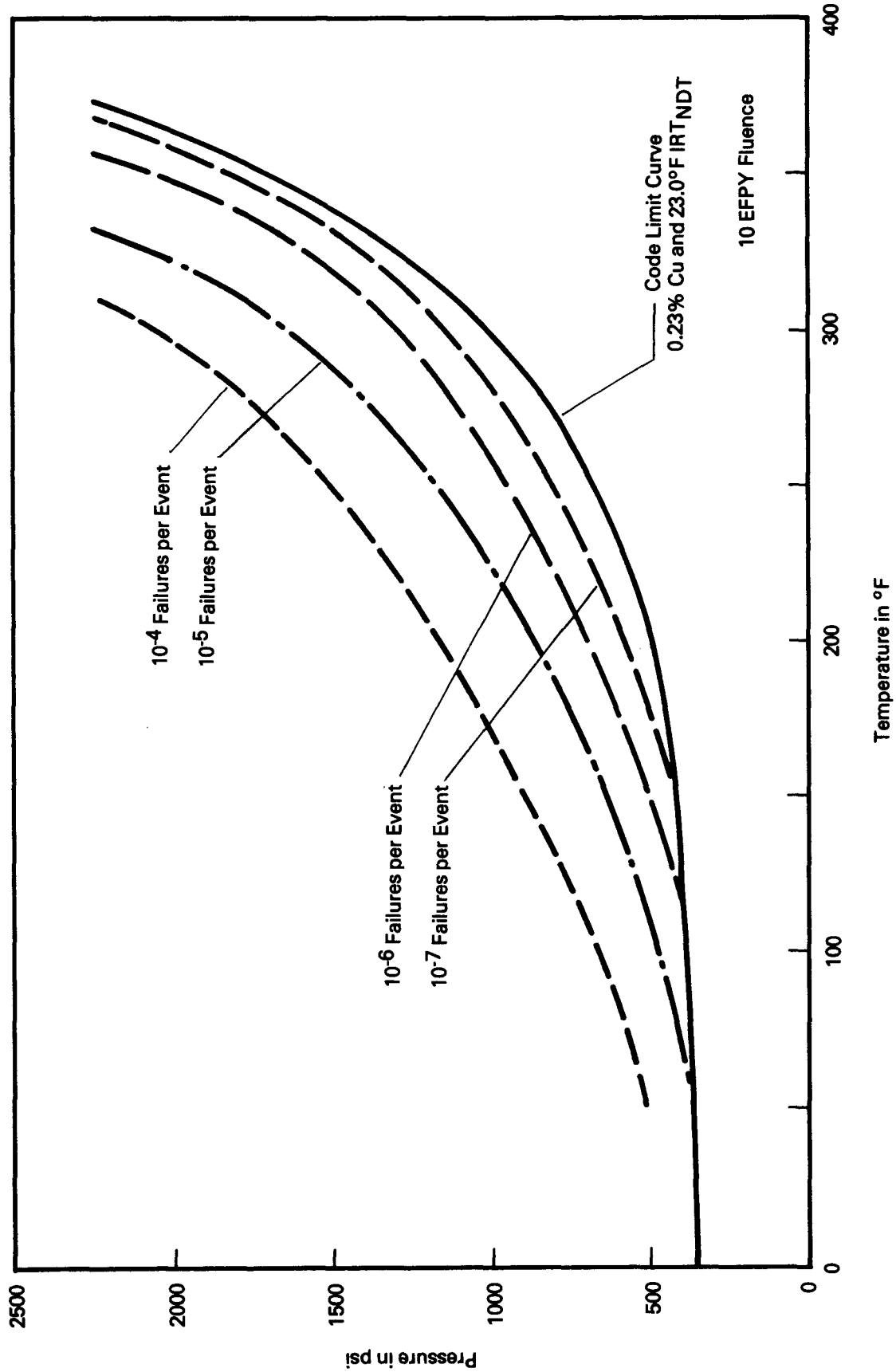

Figure 5.1: Constant Failure Rate and Code-Allowable Pressure Temperature Paths for Reactor Shutdown at 10 EFPY Fluence

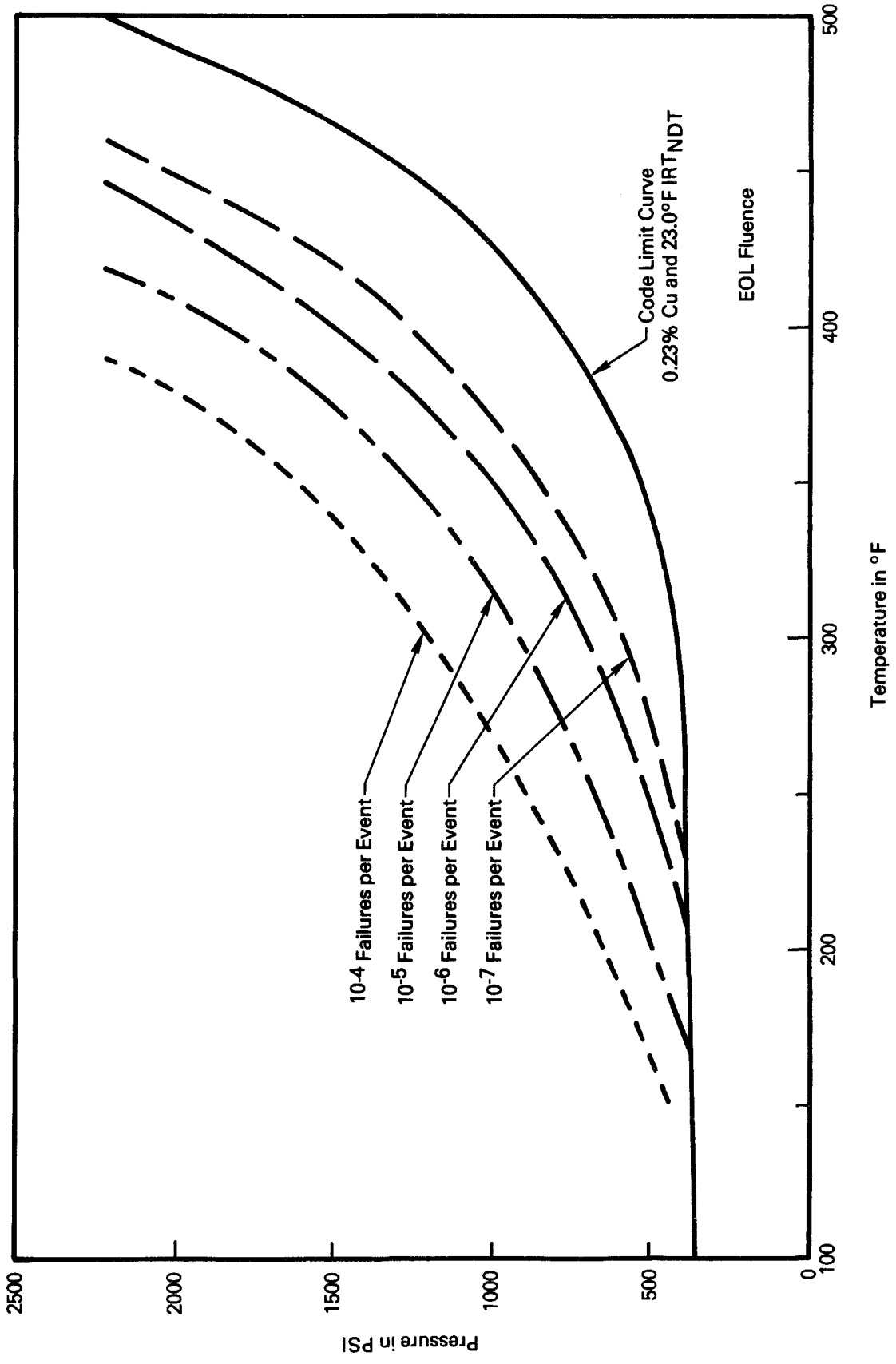

Figure 5.2: Constant Failure Rate and Code-Allowable Pressure Temperature Paths for Reactor Shutdown at EOL Fluence

probability and the relative margins of safety established by the code limits for startup and shutdown operation.

5.1.2 Sensitivity Studies for Shutdown Operation

The variables included in the parametric studies for normal shutdown operation are flaw orientation, flaw location, startup condition, flaw distribution, minimum detectable flaw size, copper content, and K_{IC} range. Except for the particular variable under consideration during a parametric study, the variables used in each analysis are those described in Section 4.4 for the reference variable condition.

5.1.2.1 Flaw Orientation

Because the beltline regions of many reactor pressure vessels contain both longitudinal and circumferential welds, a parametric study was completed to determine the relative contribution to failure probability from longitudinally and circumferentially oriented flaws. Flaw orientation, of course, is expected to significantly affect the calculated failure probability because the calculated pressure stress acting on a flaw which is embedded in a longitudinal beltline weld is twice that acting on a flaw located in a circumferential beltline weld.

Figure 5.3 presents a comparison of the pressure/temperature paths that correspond to shutdown operation at a constant failure rate of 10^{-5} failures per event for a vessel having either all longitudinal or all circumferential welds in the beltline region. The results are for a neutron-fluence level corresponding to 10 EFPY of operation. The flaw distribution used to calculate the failure rate for circumferential welds was obtained by modifying the OCTAVIA longitudinal distribution in Figure 4.2 according to the ratio of the circumferential to longitudinal beltline weld volumes illustrated in Figures 2.1a and 2.1b, respectively. As expected, the relative position of the two curves indicates that a vessel having only circumferential beltline welds can sustain a much greater pressure at any specified temperature and failure rate.

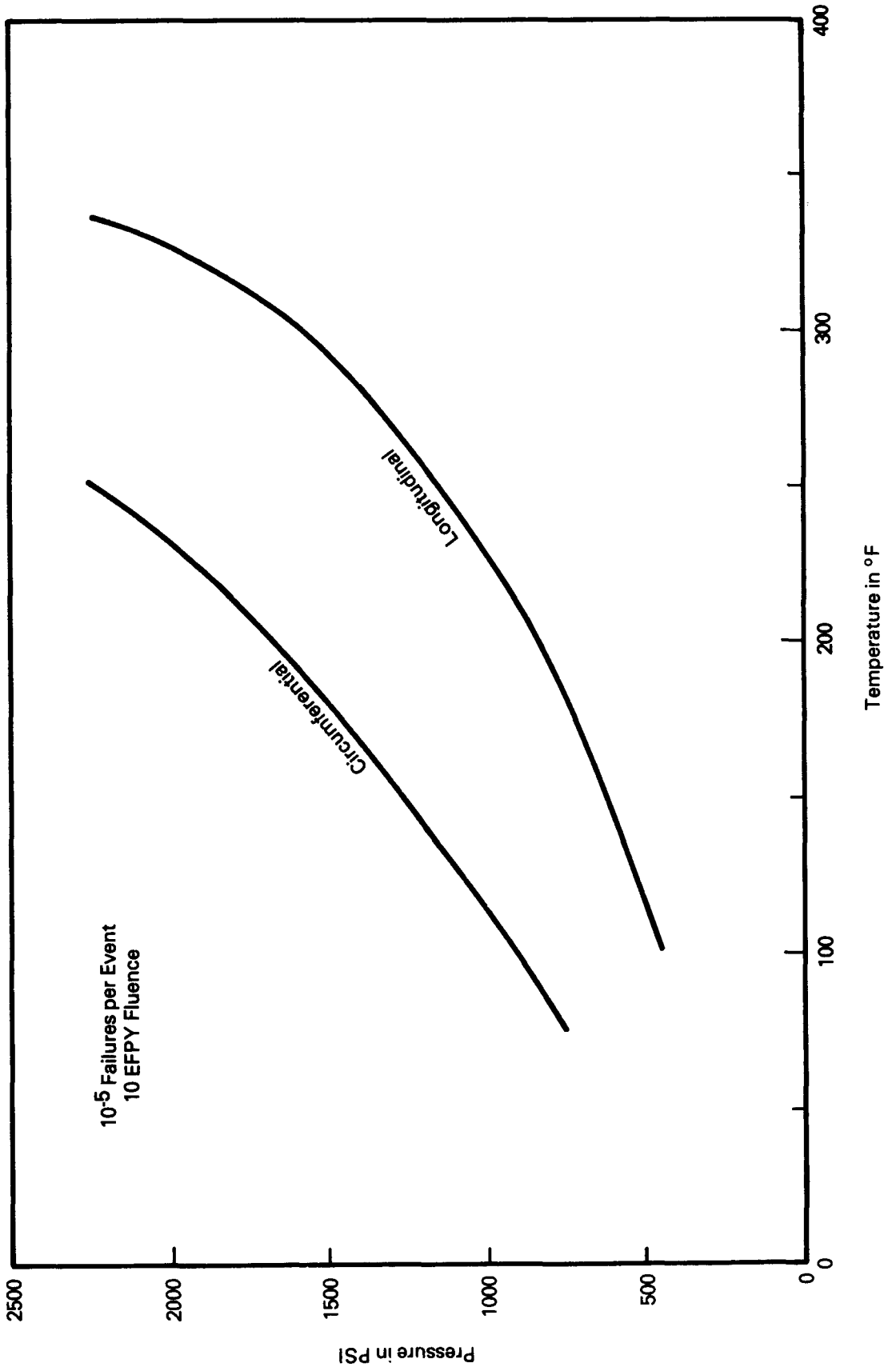

Figure 5.3: Comparison of Constant Failure-Rate Paths For Beltline Regions Having Only Circumferential Welds and Only Longitudinal Welds

To obtain a numerical estimate of the relative contribution to failure probability of longitudinal and circumferential welds, the failure rate for a longitudinal weld was calculated at several points along the 10^{-5} failure-rate path for circumferential weld volume. The results indicate that, at a specified pressure/temperature point, the failure rate for a vessel with only longitudinal welds is approximately 100 times greater than that for a vessel with only circumferential welds in the beltline. However, this factor of 100 is an upper bound. Because the circumferential-weld volume is a small contributor to failure rate compared to the longitudinal-weld volume, a more accurate estimate would be obtained by adding the failure-rate contribution from the base metal volume and associated flaw distribution to the calculated failure rate associated with the circumferential-weld volume.

The results, however, are adequate to show that the longitudinal-weld volume dominates the calculated failure rate in a vessel beltline having both weld orientations. For this reason, the analyses in this report typically are based on the beltline configuration illustrated in Figure 2.1a, where only the longitudinal-weld volume is used to determine failure rate.

5.1.2.2 Flaw Location and Startup Condition

The results contained in this report are based on the assumption that the flaw always extends into the vessel wall from the inside surface. However, flaws are likely to be distributed throughout the vessel wall. Flaw location influences calculated failure rate because the values of neutron fluence, thermal, and residual stress, as well as the modifying function, F_i, in equation (1), vary through the vessel wall. Startup and shutdown operations also are evaluated as failure-rate parameters because they are coupled with flaw location. The coupling exists because the magnitude and sign of the thermal stress change within the vessel wall as a function of startup and shutdown operations.

To determine how calculated failure rate is affected by flaw location and startup and shutdown operations, pressure/temperature paths that correspond to operation at a constant failure rate were determined for the following conditions:

(1) Shutdown - flaw at vessel inner surface only
(2) Shutdown - flaw equally likely at vessel inner or outside surface
(3) Startup - flaw at vessel inner surface only
(4) Startup - flaw at vessel outside surface only
(5) Shutdown - flaw at vessel outside surface only

Although other combinations of startup and shutdown operations and flaw location could have been examined, these five conditions illustrate the influence of the two parameters on failure rate, show the interaction of the parameters, and identify the dominant conditions.

The pressure/temperature paths associated with the five startup, shutdown, and flaw combinations are presented in Figure 5.4. The results represent startup or shutdown operation at a constant failure rate of 10^{-5} failures per event for a neutron fluence corresponding to EOL.

Several observations can be made from the results presented in Figure 5.4. First, the upper bound of the five conditions is the pressure/temperature path developed for shutdown operation of a vessel having an outside flaw only; the lower bound corresponds to shutdown operation of a vessel having only an inside flaw. The shutdown bounding conditions are expected because during shutdown an outside flaw experiences the lowest fluence and thermal stress, while an inside flaw is subjected to the highest fluence and thermal stress.

In contrast to the bounding curves associated with shutdown, the two pressure/temperature paths developed for startup operation with (respective) inside and outside flaw locations lie quite close to each other. During startup a flaw located at the inside surface is subject to relatively high fluence and low thermal stress, compared to an outside flaw where the fluence is low but the thermal stress is high. Thus for startup operation, fluence and thermal stress are parameters that compensate rather than reinforce each other with respect to calculated failure rate. The proximity of the two startup curves indicates that the fluence/thermal stress compensation is nearly 1 to 1 in this instance.

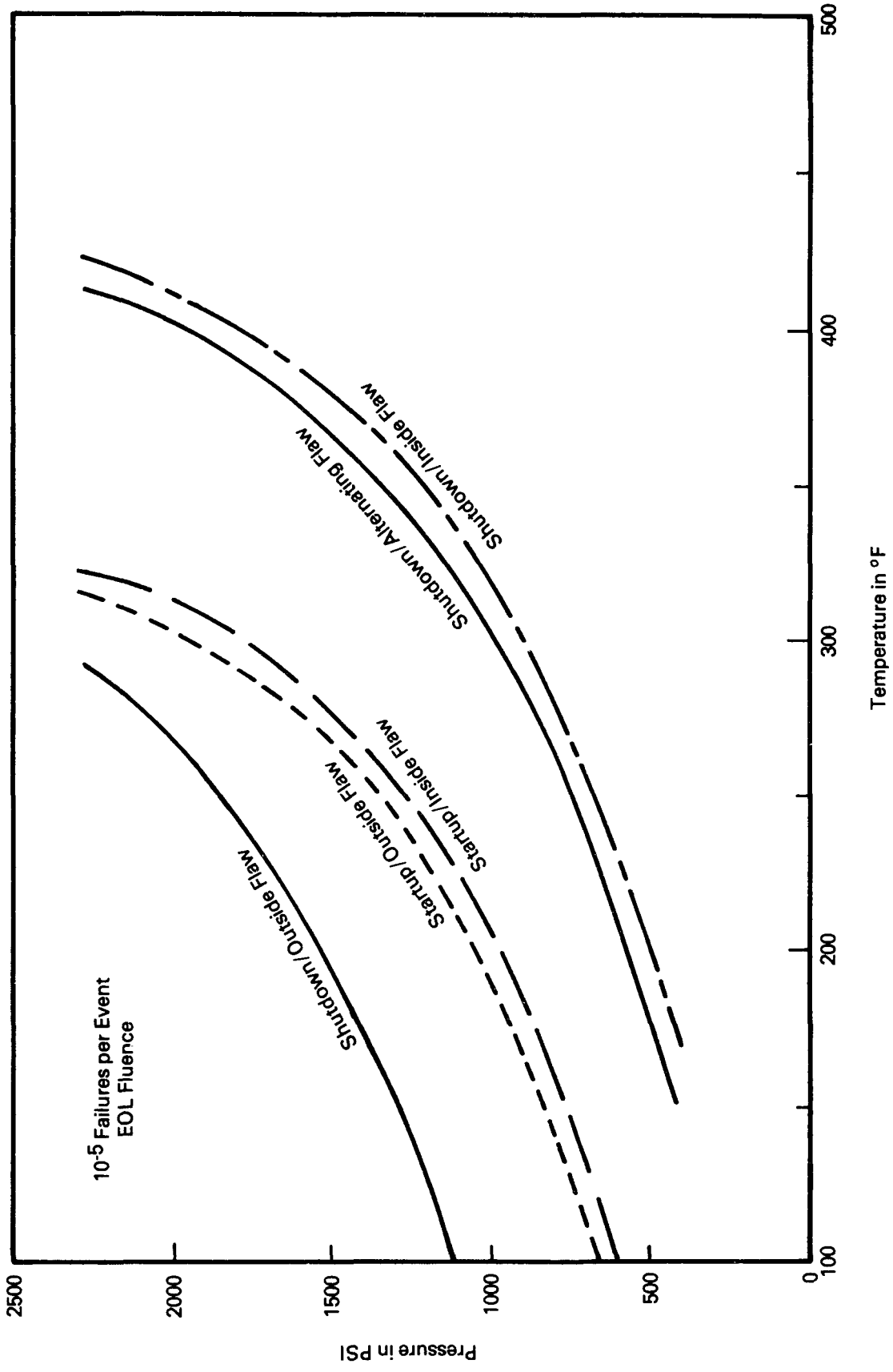

Figure 5.4: Effect of Flaw Location and Startup/Shutdown Condition on Constant Failure-Rate Pressure/Temperature Path at EOL Fluence.

Finally, both startup and shutdown operations were analyzed using the assumption that the vessel would have both inside and outside surface flaws, each of which was equally likely to occur. The probability that any specific size flaw would occur remained the same as that used for the single-flaw analyses.

The resultant pressure/temperature path for shutdown operation is shown in Figure 5.4 as the second curve from the right. As might be expected by the relative positions of the two shutdown curves with single inside and outside flaw locations, the alternating flaw condition during shutdown is dominated by the inside flaw location. The pressure/temperature path corresponding to the alternating flaw condition for startup is not shown in Figure 5.4 but lies between the two startup paths for the single-flaw location. This location, of course, indicates that the inside and outside surface flaws contribute approximately the same amount to failure probability during startup.

The results in Figure 5.4 indicate that shutdown operation and inside flaw location are the operational condition and flaw location that dominate calculated failure rate in the startup/shutdown sequence. Further, the results obtained for startup and shutdown operation are sufficient to indicate that the inside surface flaw condition also dominates the calculated failure rate for the three remaining operational events. For this reason, an inside surface flaw typically is used throughout this report in the analyses of all the operational events; shutdown operation is used to represent the startup/shutdown operational sequence. The use of more precise models for these variables would not significantly alter the calculated results.

5.1.2.3 Flaw Distribution

The flaws of interest in this generic fracture-mechanics evaluation are those that are undetected and remain in the vessel. Consequently, few data are available to form a precise quantitative definition of flaw distribution, and parametric studies were conducted to determine the sensitivity of calculated failure rate to flaw distribution. The OCTAVIA end-of-life and Marshall preservice flaw distributions shown in Figure 4.2 were used in the sensitivity study. These two distributions were chosen because (1) they bound the

distributions that typically are used in analyses of the rates of vessel failure, and (2) intuition suggests that either distribution could reasonably be expected to exist in a vessel at some point in the operating life of the vessel.

Figures 5.5 and 5.6 present the constant 10^{-5} failure-rate pressure/temperature paths calculated for the two distributions at neutron-fluence levels corresponding to 10 EFPY and EOL, respectively. To obtain a numerical estimate of the effect of flaw distribution on failure rate, failure rates were calculated using the OCTAVIA distribution at several points along the 10^{-5} failure-rate curves obtained from the Marshall preservice distribution. The results indicate that the failure rates obtained by using the OCTAVIA flaw distribution are approximately an order of magnitude higher than those obtained using the Marshall preservice flaw distribution.

The results shown in Figures 5.5 and 5.6 suggest that the failure rate for the startup/shutdown sequence is mildly sensitive to the range of flaw distributions evaluated in this report. The calculated results also indicate that fatigue-crack growth is a small contributor to failure rate for the startup/shutdown sequence. This conclusion is based on the observation in Figure 4.2 that the maximum predicted relative fatigue-crack-growth distribution, designated as Marshall EOL, lies between the two distributions used in the sensitivity study. Based on the expected relative position of fatigue-crack-growth distribution at 10 EFPY and EOL, it appears that fatigue-crack growth contributes signficantly less than an order of magnitude to failure rate.

5.1.2.4 Minimum Detectable Flaw Size

Reactor pressure vessels are volumetrically inspected periodically during fabrication and subsequent service. The methods used for these inspections make it likely that flaws below some minimum size will not be detected. The effect of a minimum detectable flaw size on calculated failure rate is of interest; it suggests a desirable minimum level of inspection sensitivity to ensure vessel integrity. By altering the minimum flaw size in the discrete representation of the OCTAVIA flaw distribution, a sensitivity study was

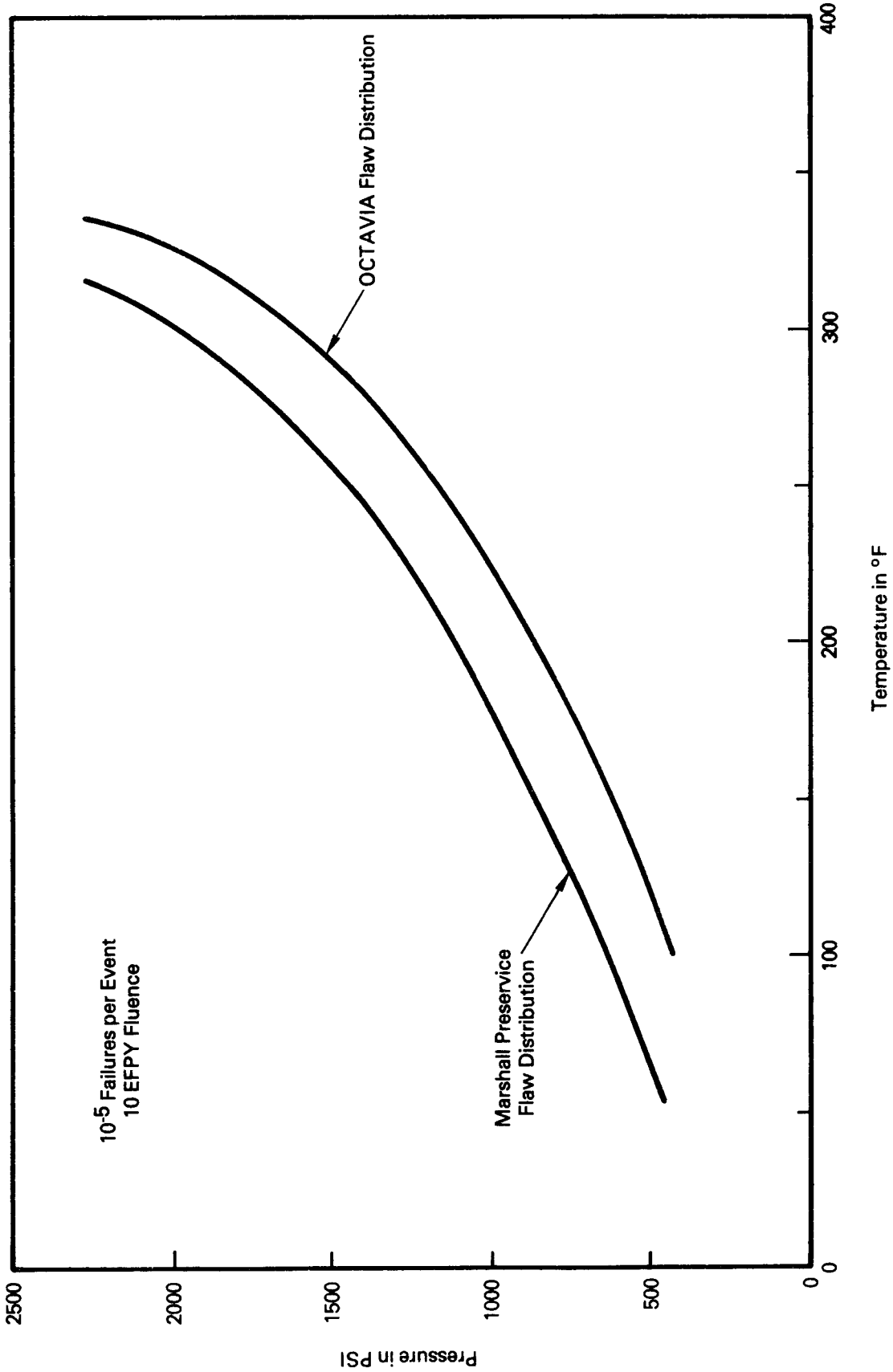

Figure 5.5: Comparison of 10^{-5} Constant Failure-Rate Pressure/Temperature Paths for OCTAVIA EOL and Marshall Preservice Longitudinal Flaw Distributions at 10 EFPY Fluence.

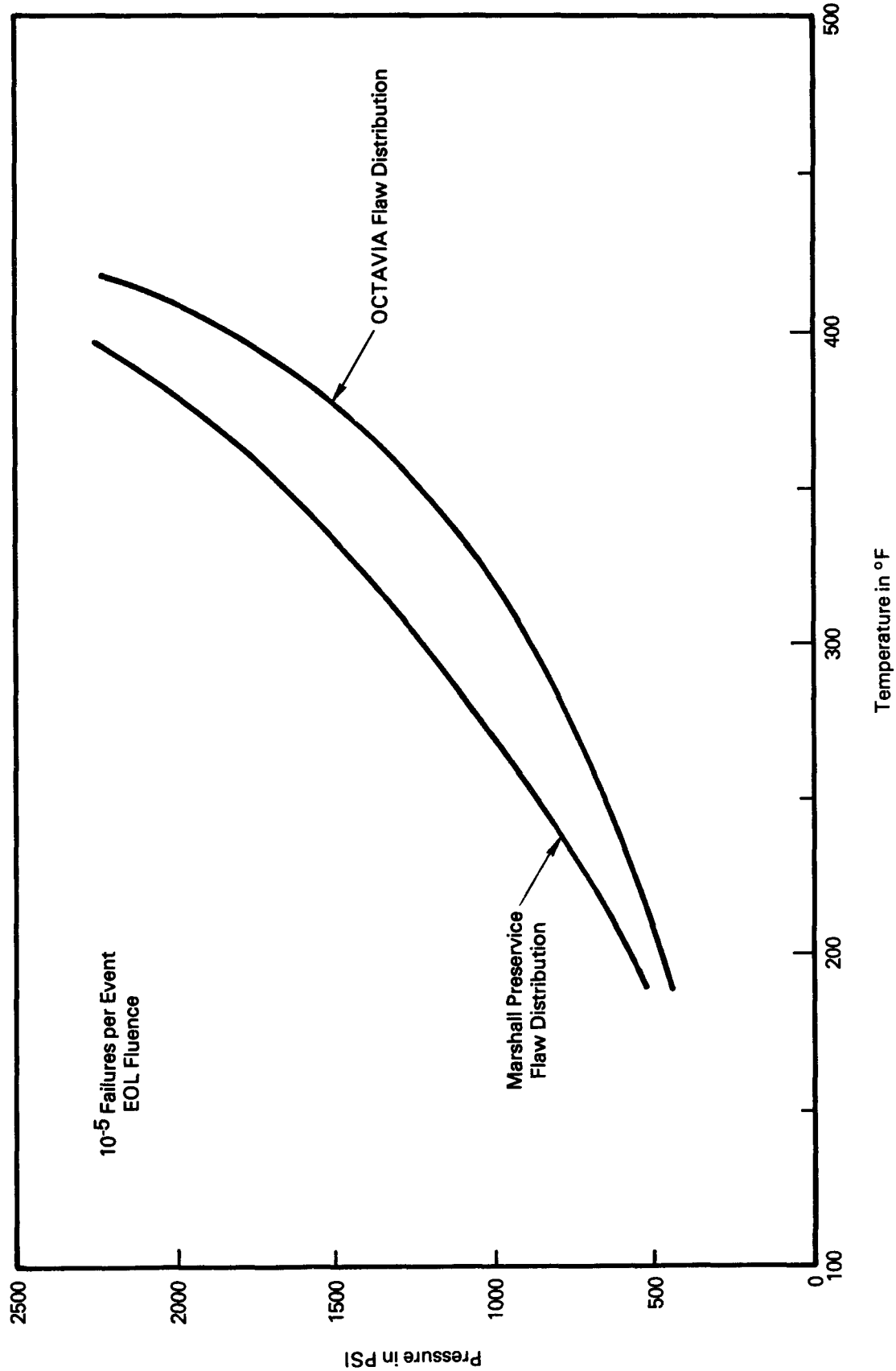

Figure 5.6: Comparison of 10^{-5} Constant Failure-Rate Pressure/Temperature Paths for OCTAVIA EOL and Marshall Preservice Longitudinal Flaw Distributions at EOL Fluence.

conducted assuming that 0.125-in., 0.25-in., 0.5-in., and 1.0-in. flaws are almost always present and undetected in the vessel beltline.

The results indicate that the calculated failure rate for the startup/shutdown sequence is insensitive to the minimum detectable flaw sizes of 0.125 in., 0.25 in., and 0.5 in. However, when 1.0-in. flaws are assumed to be undetectable, the calculated failure rate increases by approximately two orders of magnitude. The results were obtained at a neutron-fluence level corresponding to 10 EFPY of operation.

5.1.2.5 Copper Content

As described in Section 4.4, the copper distribution for the reference variable condition represents the variation in copper content through the beltline weld volume of operating PWRs. However, two additional distributions are important for a generic study of reactor-vessel integrity. These additional distributions are (1) a distribution associated with newer vessels, where copper content is reduced and less variable than that in operating PWRs and (2) constant copper content used to construct ASME code pressure/temperature limits for startup and shutdown operations. Parametric studies were completed to define the relative effect of the various copper distributions on calculated failure rate.

Results from the sensitivity studies are illustrated in Figures 5.7 and 5.8 for neutron-fluence levels corresponding to 10 EFPY and EOL operations, respectively. Pressure/temperature paths corresponding to a calculated constant failure rate of 10^{-5} failures per event are presented in each figure for two normal distributions and four constant copper values. The distribution representing operating PWRs has a mean, μ, of 0.23% and a standard deviation, σ, of 0.07%. The distribution associated with newer plants has μ equal to 0.12% and σ equal to 0.012%. The four constant values of copper content are 0.12, 0.15, 0.23 and 0.35%. The normal distribution used for newer plants is an estimate based on upper limits for copper content that are typically used in material specifications. The constant values of copper content of 0.12, 0.15, 0.23, and 0.35% represent, respectively, the estimate of the mean of the new plant distribution, the two-sigma limit for the new

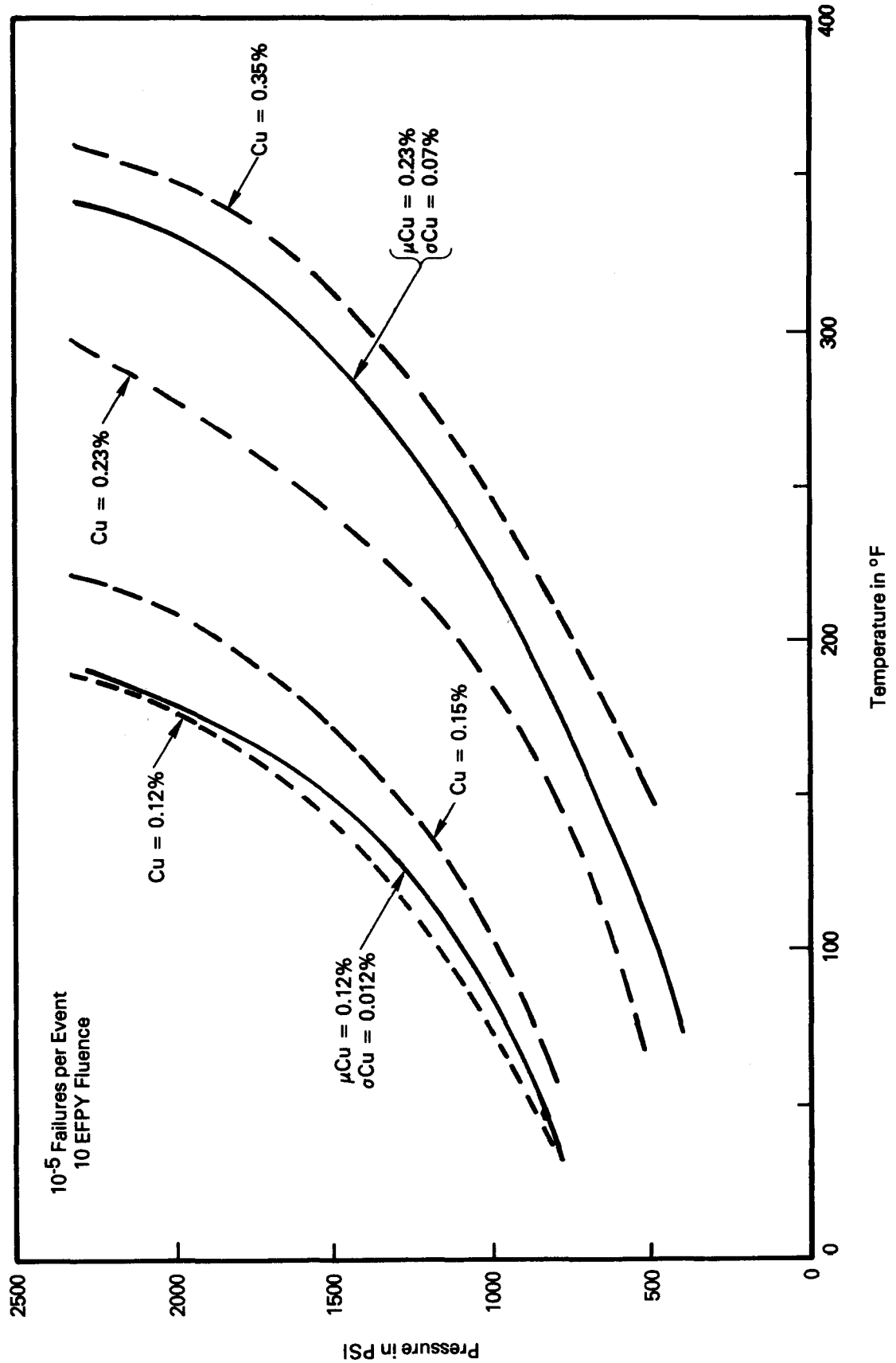

Figure 5.7: Effect of Copper Content and Distribution on Constant 10^{-5} Failure-Rate Pressure/Temperature Paths at 10 EFPY Fluence

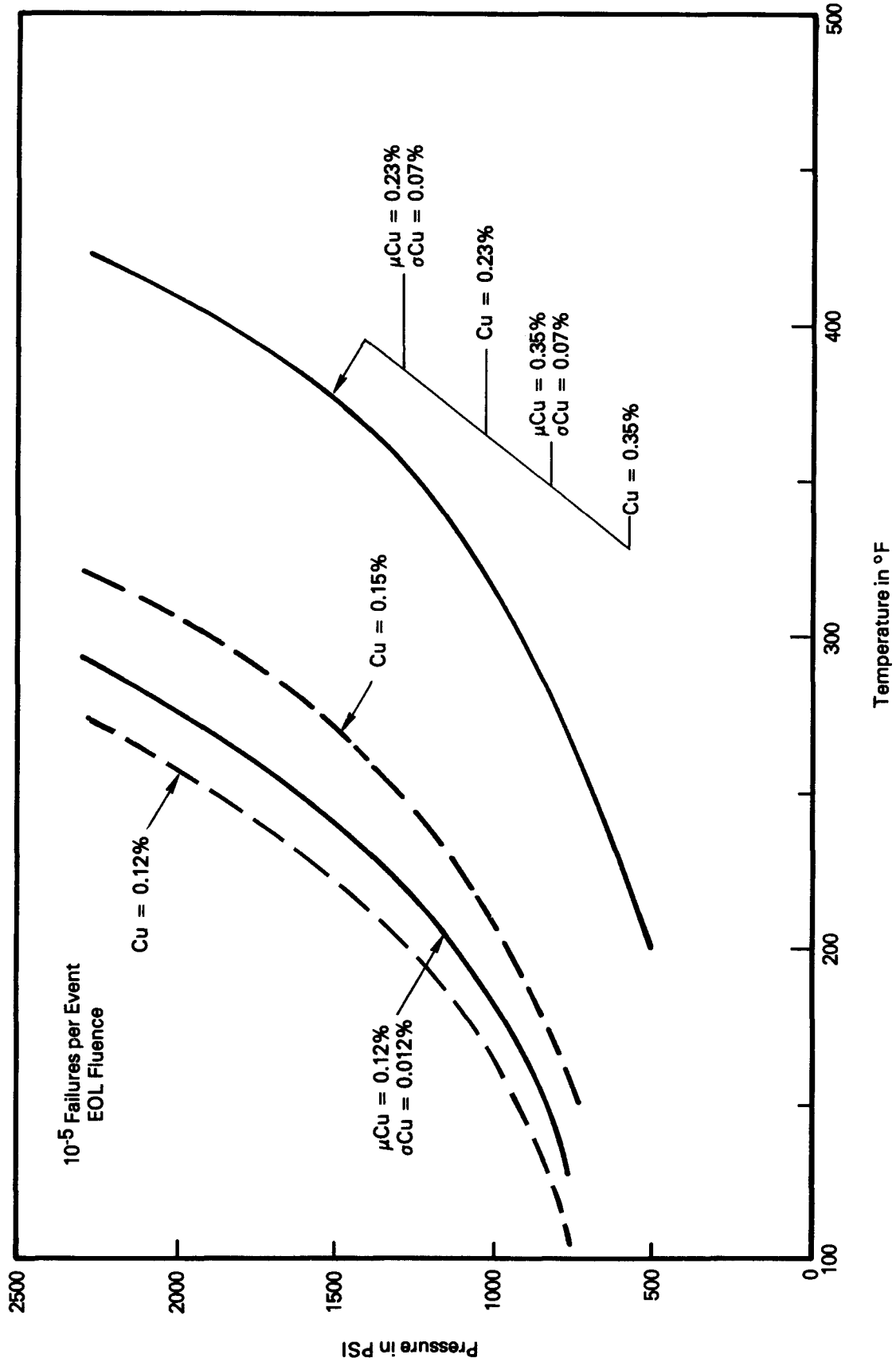

Figure 5.8: Effect of Copper Content and Distribution on Constant 10^{-5} Failure-Rate Pressure/Temperature Paths at EOL Fluence

plant distribution, the mean for the operating plant distribution, and the upper-limit copper content used in Regulatory Guide 1.99 (Ref. 15).

The results shown in Figures 5.7 and 5.8 indicate that the constant failure-rate curves associated with the two normal distributions are bounded by the curves obtained for constant values of copper content representing the mean and the mean plus approximately two standard deviations for the respective distributions. For the EOL-fluence level and the higher copper contents representative of operating PWRs, the curves for the mean, upper limit, and normal distributions are coincident. The concidence occurs because the combination of high copper content and fluence dictates that $(T\text{-}RT_{NDT})$ is in the lower part of the fracture-toughness curve in Figure 4.3. Here, the value of K_{IC} does not change rapidly with changes in RT_{NDT}; consequently, the calculated failure rates are relatively insensitive to copper content and fluence in this range.

In contrast, the results in Figure 5.7 show that failure rate is quite sensitive to the copper content at fluences associated with 10 EFPY of operation. This sensitivity exists because the combination of copper content and fluence results in values of $(T\text{-}RT_{NDT})$ that are in the transition region of Figure 4.3. In this region, K_{IC}--and hence the failure rate--is quite sensitive to changes in RT_{NDT}.

5.1.2.6 K_{IC} Range

As described in Chapter 4, the variation of the material-fracture toughness, K_{IC}, is modeled by a standard deviation that is 10% of the mean value obtained from equations (2) and (3). For the reference variable condition, the allowable range of material-fracture toughness is

$$(\bar{K}_{IC} - 3\sigma) \leq K_{IC} \leq (\bar{K}_{IC} + 3\sigma)$$

However, because the estimates of standard deviation and range of K_{IC} are based on limited data, a parametric study was performed at the 10 EFPY-fluence level to estimate the sensitivity of calculated failure rate to the range of

allowable K_{IC}. Several additional ranges of K_{IC} were evaluated; these included

$$\bar{K}_{IC};\ (\bar{K}_{IC} \pm 1\sigma);\ (\bar{K}_{IC} \pm 2\sigma);\ (\bar{K}_{IC} \pm 3\sigma);\ \text{and}\ o \leq K_{IC} \leq (\bar{K}_{IC} \pm 3\sigma)$$

The results from the sensitivity studies indicate that failure rate increases as the range of fracture toughness increases from a constant value of $\bar{K}_{IC}$ to the ranges $(\bar{K}_{IC} \pm 1\sigma)$ amd $(\bar{K}_{IC} \pm 2\sigma)$. Over this range of K_{IC} the increase in failure rate was less than a factor of 5 at higher temperatures in the transition temperature region and was approximately equal to a factor of 10 at lower temperatures in the transition region. The calculated failure rates remained essentially constant throughout the entire transition temperature region for the fracture toughness ranges of $(\bar{K}_{IC} \pm 2\sigma)$, $(\bar{K}_{IC} \pm 3\sigma)$, and $o \leq K_{IC} \leq (\bar{K}_{IC} + 3\sigma)$.

5.2 Normal Full-Power Operation

This section presents the calculated failure rates for the reference variable condition and various parametric studies associated with full-power operation in the upper-shelf temperature region. The failure rates are calculated at fluence levels corresponding to 10 EFPY and EOL operation.

As Reference 15 and equation (3) specify, the fracture resistance of irradiated pressure-vessel steels in the upper-shelf temperature region can be expressed as a function of the initial unirradiated upper-shelf CVN absorbed energy and a decrease in this initial value as a result of neutron irradiation. Consequently, the calculated failure rates in the section are presented as a function of both the unirradiated and irradiated CVN upper-shelf absorbed energies. This presentation facilitates comparison of the results with the minimum absorbed energy values specified for the beltline region materials by Appendix G to 10 CFR Part 50, namely, 75 ft-lb for unirradiated material and 50 ft-lb for irradiated material.

5.2.1 Reference Variable Condition

Figures 5.9 and 5.10 present the calculated failure rate vs upper-shelf energy at neutron-fluence levels corresponding to 10 EFPY and EOL, respectively, for normal operation at 2250 psi and 550°F and the reference variable condition. For full-power operation, the reference variable condition includes an assumed thermal stress equal to zero.

The upper-shelf energies are represented in the figures by two scales on the abcissa. The upper scale on the abcissa is the orginal unirradiated upper-shelf energy. For convenience, the lower scale provides a reference for evaluating the condition of the irradiated material and represents the mean irradiated upper-shelf energy at a quarter of the wall thickness from the inside surface of the vessel, assuming a copper content of 0.23%. This representation is used to define irradiated upper-shelf energy because a single value cannot be defined when fracture toughness, flaw depth, and copper content are treated as random variables.

For a neutron-fluence level corresponding to 10 EFPY, Figure 5.9 indicates failure rates of less than 10^{-6} when the unirradiated and irradiated upper-shelf energies are greater than approximately 45 and 29 ft-lbs, respectively. For a neutron-fluence level corresponding to EOL, the calculated failure rates are less than 10^{-6} when the unirradiated and irradiated upper-shelf energies are greater than approximately 55 and 29 ft-lbs, respectively.

A comparison of the calculated relationship between failure rate and upper-shelf energy in Figures 5.9 and 5.10 can be used to illustrate the relative margins against fracture provided by the 75- and 50-ft-lb limits set by Appendix G to 10 CFR 50 for unirradiated and irradiated material, respectively. For example, the figures indicate that an irradiated upper-shelf energy greater than approximately 29 ft-lb corresponds to a failure rate of less than 10^{-6} failures per event. This is significantly less than the specified 50 ft-lb. The results in Figure 5.10 indicate that the initial unirradiated upper-shelf energy corresponding to a failure rate less than 10^{-6} failure per event must be at least 55 ft-lb; this value is significantly less than the specified 75 ft-lb. However, these indicated correlations

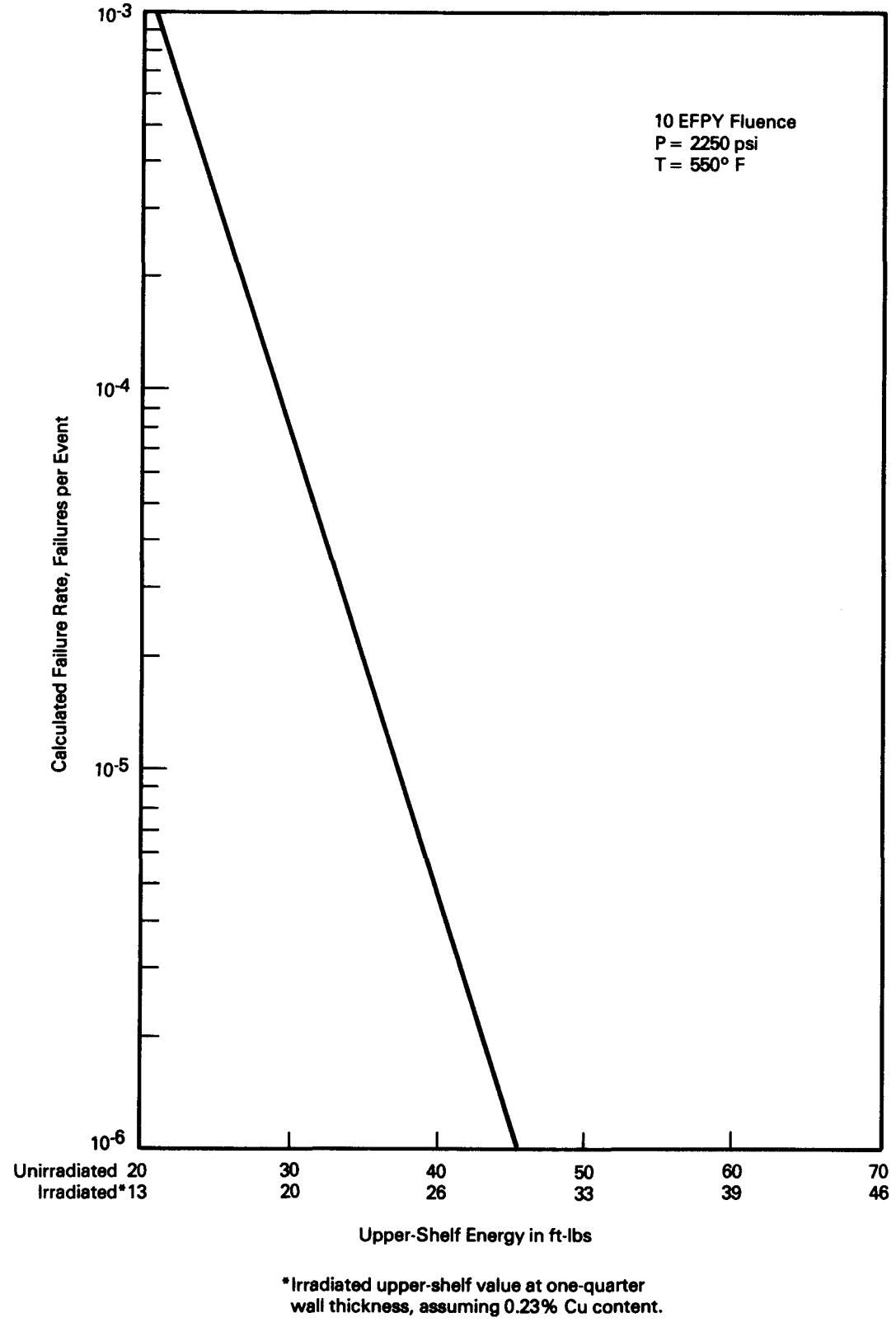

Figure 5.9: Reference Case Failure Rate vs Upper-Shelf Energy For Full-Power Operation at 10 EFPY Fluence

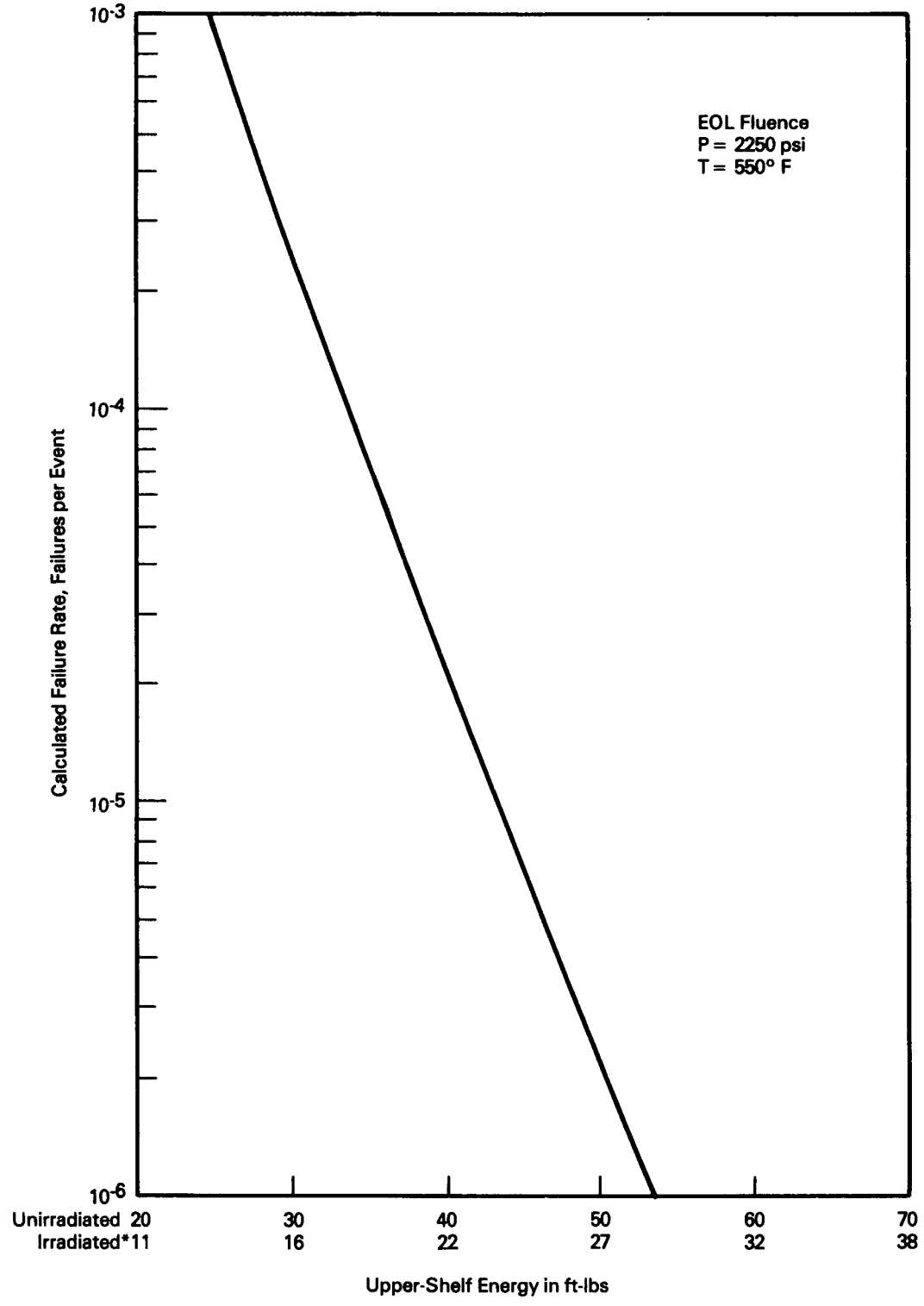

Figure 5.10: Reference Case Failure Rate vs Upper-Shelf Energy For Full-Power Operation at EOL Fluence

between failure rate and single specified values of upper-shelf energy are not exact and depend on variables such as flaw distribution, assumed single values for copper content, and the irradiation damage model. Different input for these variables would shift the position of the calculated curves relative to the requirements of Appendix G to 10 CFR 50 and modify the indicated margins.

The results from the parametric studies in the following sections can be used to judge the influence of several variables on the relationship between failure rate and upper-shelf energy.

5.2.2 Normal Full-Power-Operation Sensitivity Studies

The variables included in the parametric studies for normal full-power operation in the upper-shelf temperature region are flaw distribution, minimum detectable flaw size, copper content, and thermal stress. Except for the particular variable being evaluated during a parametric study, the variables used in each analysis are those described in Section 4.4 for the reference variable condition.

5.2.2.1 Flaw Distribution

Studies were performed to determine the sensitivity of calculated failure rates to the assumed flaw distribution in the upper-shelf temperature region. As in the sensitivity studies for normal startup and shutdown operation, the OCTAVIA EOL and the Marshall preservice flaw distributions were used to indicate the sensitivity of calculated failure rates to significantly different assumed flaw distributions. To estimate the effect of fatique crack growth on failure rate over the design life of a PWR, the failure rate also was calculated at the EOL fluence level for the Marshall EOL flaw distribution.

In Figure 5.11, the calculated failure rate vs upper-shelf energy is plotted for the OCTAVIA EOL and the Marshall preservice flaw distributions at a neutron-fluence level corresponding to 10 EFPY. There is a relatively large difference in calculated failure rates for the different flaw distributions; this difference ranges from one to two orders of magnitude. Figure 5.12

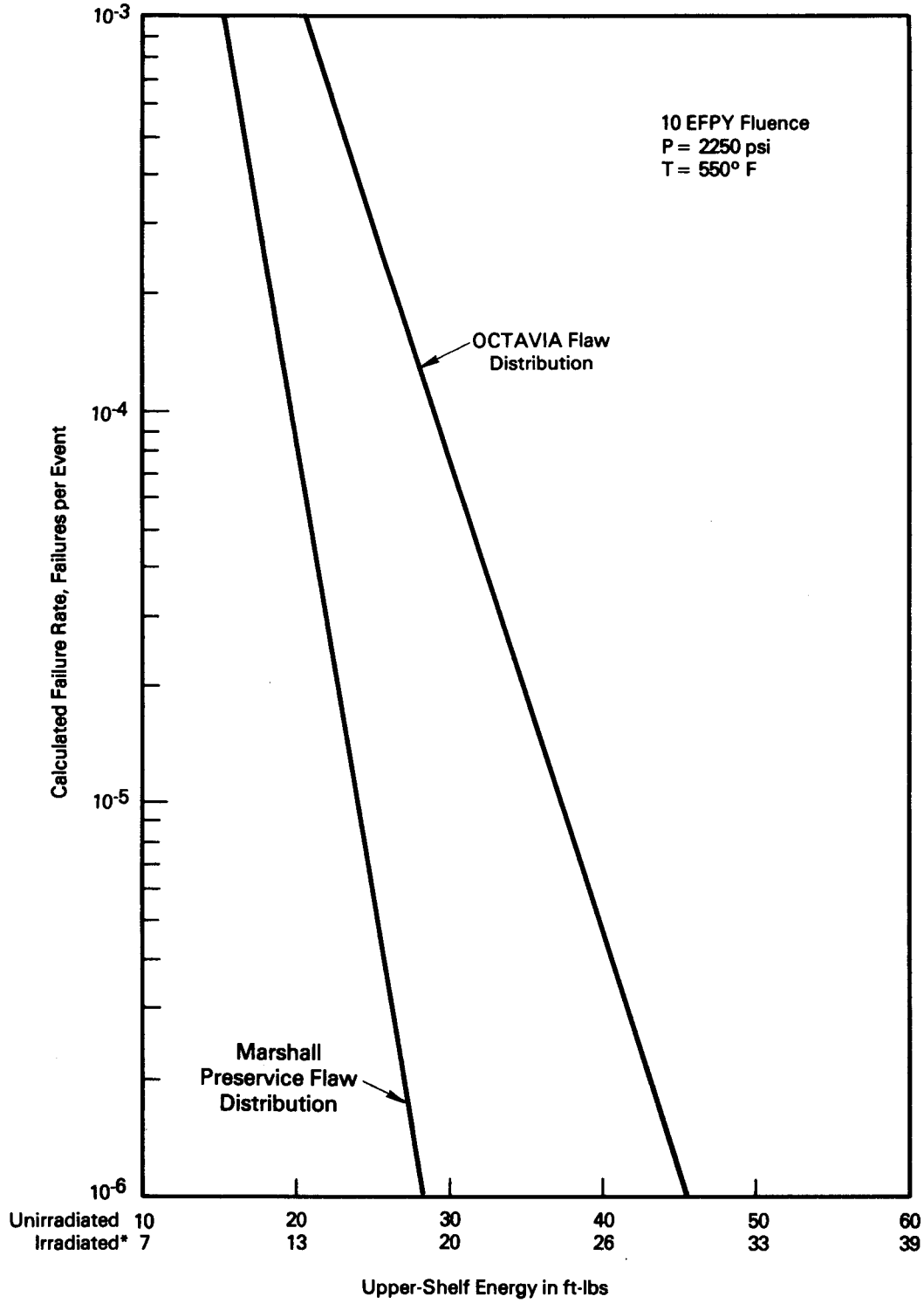

Figure 5.11: Flaw Distribution Sensitivity Study for Full-Power Operation at 10 EFPY Fluence

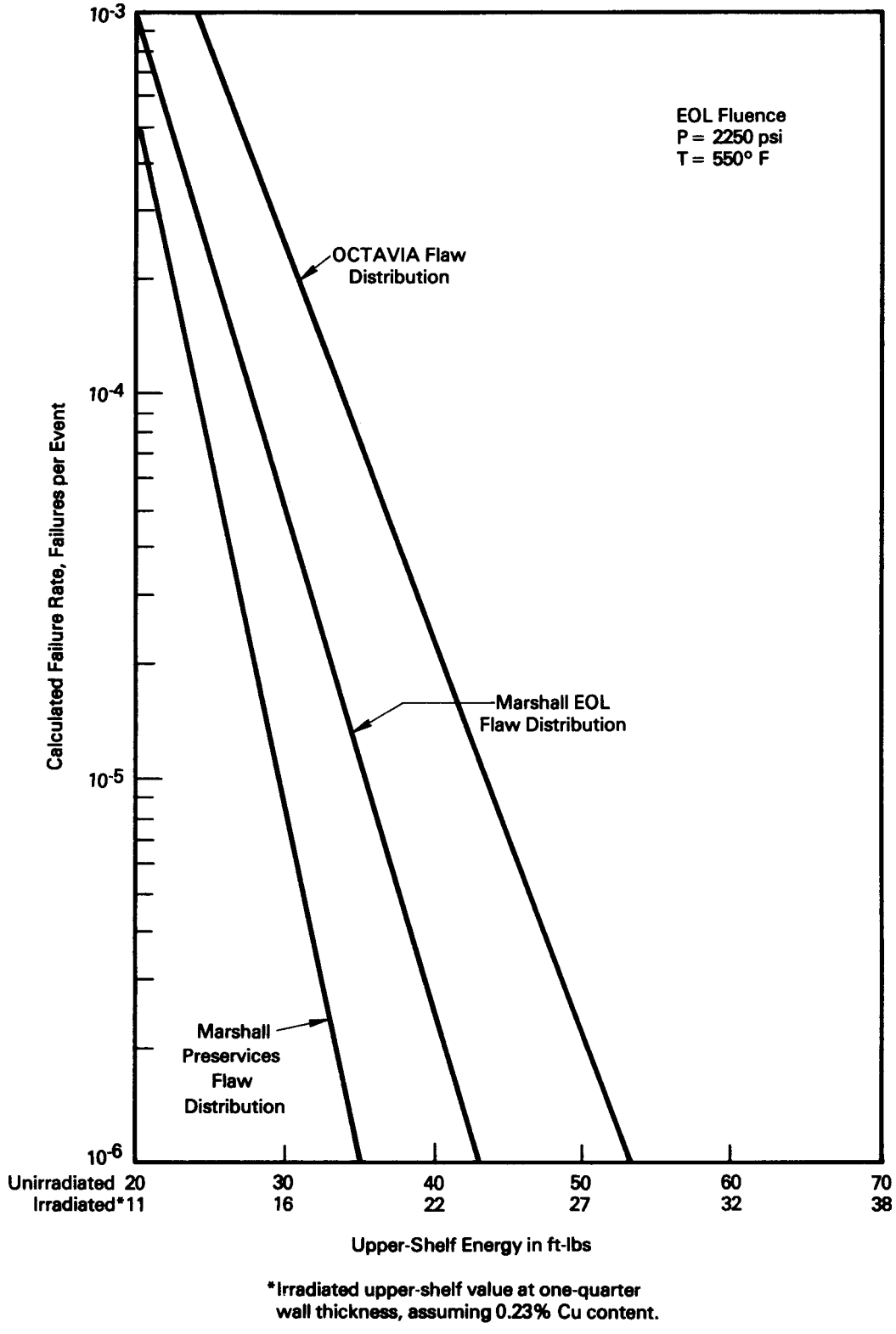

Figure 5.12: Flaw Distribution Sensitivity Study for Full-Power Operation at EOL Fluence

presents the calculated failure rate vs upper-shelf energy for the OCTAVIA and Marshall end of life, and Marshall preservice flaw distributions at a neutron-fluence level corresponding to EOL. Again the failure probability is relatively sensitive to flaw size; the calculated failure rate ranges from 10 to 100 times less for the Marshall preservice distribution than for the OCTAVIA EOL distribution. Comparison of the results obtained using the Marshall preservice and EOL flaw distributions indicates that fatigue crack growth can increase the failure rate by up to a factor of 10.

5.2.2.2 Minimum Detectable Flaw Size

Sensitivity studies were conducted to determine the effect of minimum detectable flaw size on the calculated failure rate in the upper-shelf temperature region. The discrete representation of the OCTAVIA flaw distribution was altered by assuming that 0.125-in., 0.25-in., 0.5-in., 1.0-in., and 1.5-in. flaws are almost always present and undetected in the vessel beltline. The results of these studies are presented in Figure 5.13 for a neutron-fluence level corresponding to EOL. The results shown in the figure indicate that for initial upper-shelf energies greater than 50 ft-lbs, the calculated failure rate is insensitive to undetected flaw sizes up to 1.5 in. For initial upper-shelf energies less than 50 ft-lbs, the calculated failure rate is insensitive to undetected flaw sizes up to 0.5 in. but extremely sensitive to undetected flaw sizes of 1.0 in. or greater.

5.2.2.3 Copper Content

The decrease in upper-shelf energy is mainly a function of fluence and copper content. Calculations were performed to determine the sensitivity of calculated failure rates to the same distributions of copper content that were described and evaluated in Section 5.1.2.5 for normal startup and shutdown operations. Results from the sensitivity studies are illustrated in Figures 5.14 and 5.15 for neutron-fluence levels corresponding to 10 EFPY and EOL operation, respectively. Plots of failure rate vs upper-shelf energy are presented in these figures for the normal distribution corresponding to operating plants (μ = 0.23%,

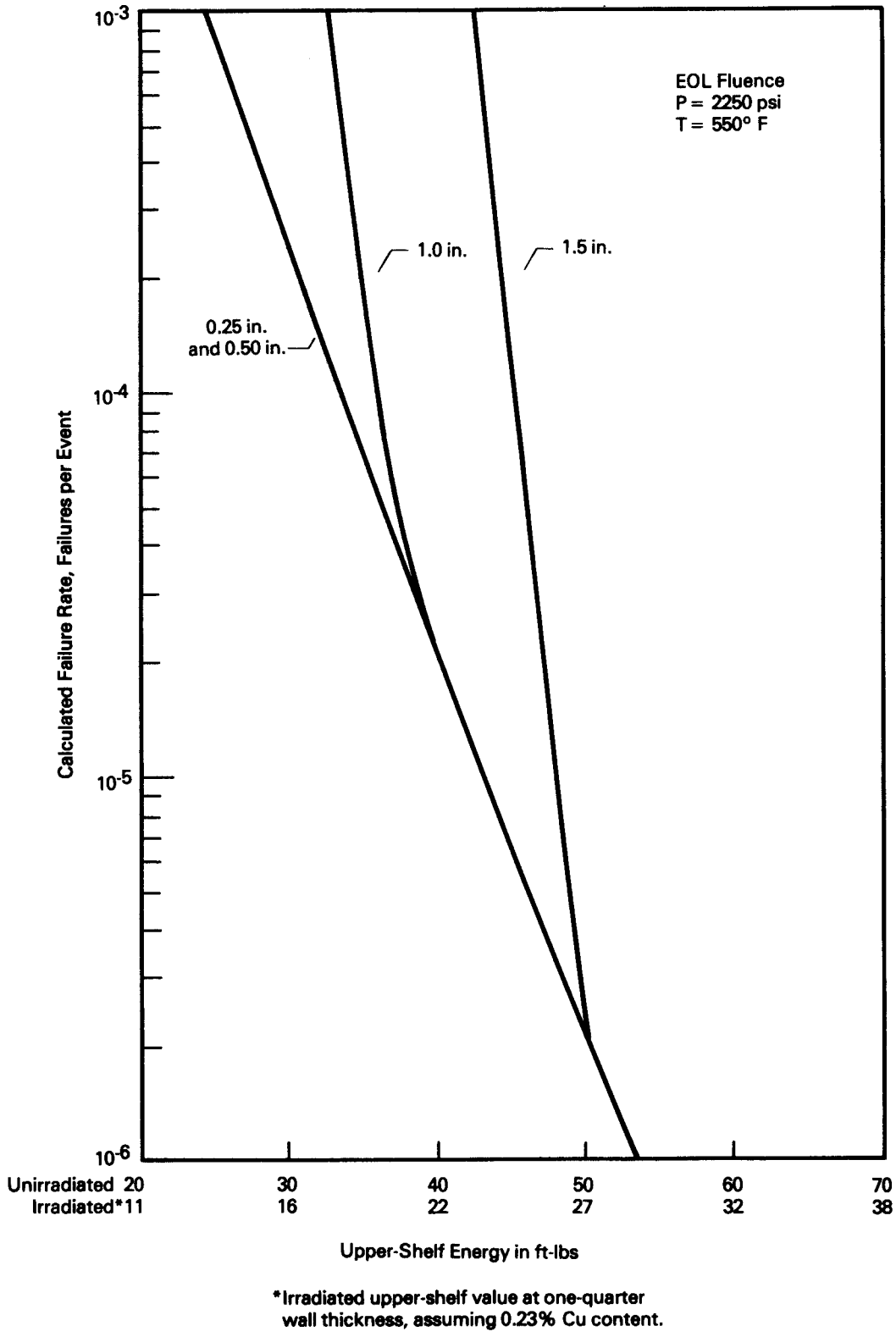

Figure 5.13: Undetected-Flaw-Size Sensitivity Study for Full-Power Operation at EOL Fluence

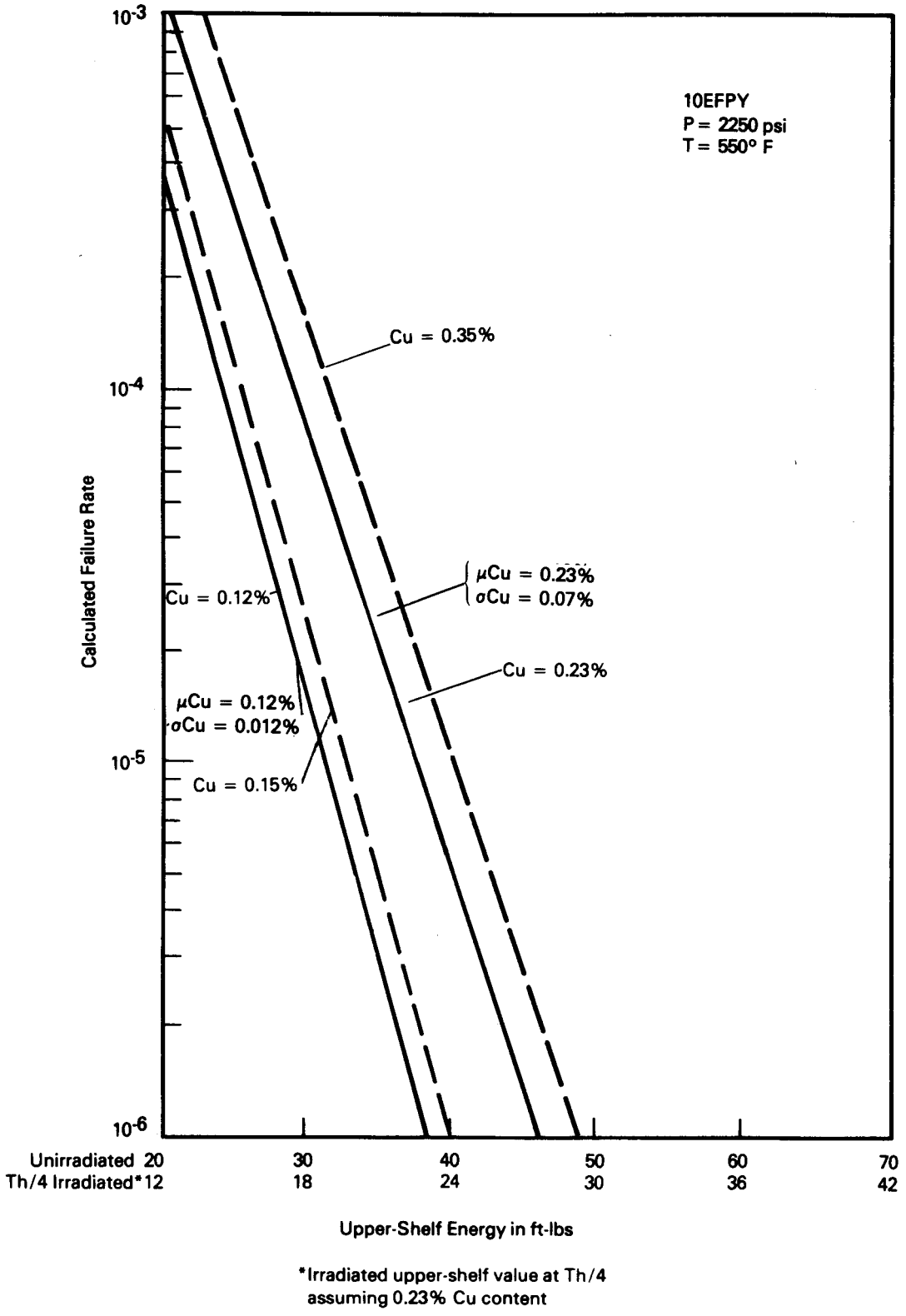

Figure 5.14: Copper-Content Sensitivity Study for Full-Power Operation at 10 EFPY Fluence

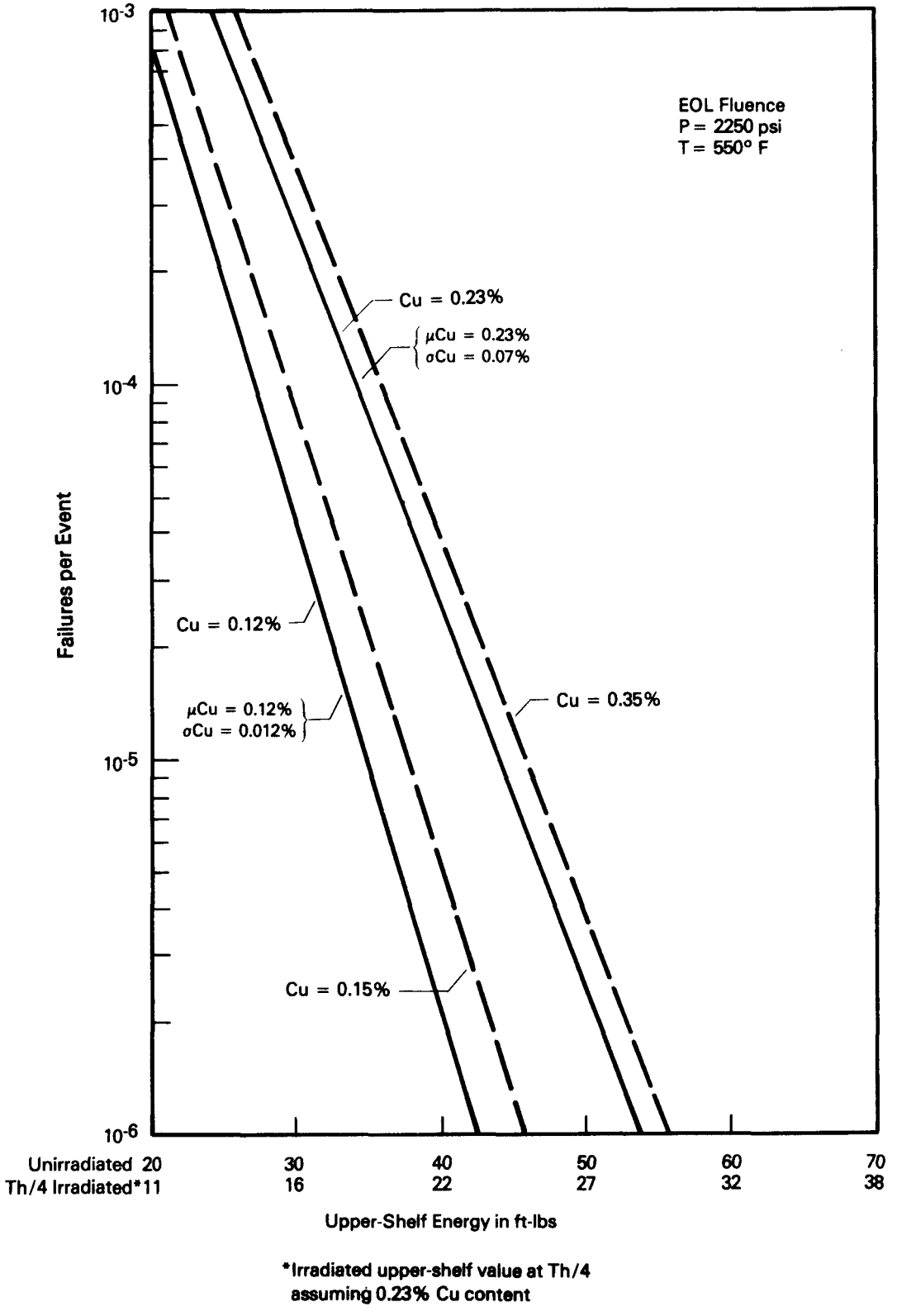

Figure 5.15: Copper-Content Sensitivity Study for Full-Power Operation at EOL Fluence

σ = 0.07%), the normal distribution assumed for new plants (μ = 0.12%, σ = 0.012%), and four constant copper contents (0.12, 0.15, 0.23, and 0.35%).

The results in Figures 5.14 and 5.15 indicate that the calculated failure rates differ by up to a factor of approximately 20 at any specified upper-shelf energy. At each fluence, the calculated failure rates associated with the two normal distributions are essentially the same as the calculated failure rates for the constant copper values corresponding to the mean of the respective distributions.

Because the computer code predicts the same drop in shelf energy at fluences greater than 3×10^{19} n/cm^2 for all copper contents greater than 0.25% (as specified in Ref. 15), the calculated failure rates for fluences greater than 3×10^{19} n/cm^2 and copper values greater than 0.25% would be expected to converge on the failure-rate curve corresponding to 0.35% constant copper value in Figure 5.15. The results indicate that calculated failure rates for normal full-power operating conditions are not as sensitive to copper content as the calculated failure rates for startup and shutdown operations.

5.2.2.4 Thermal Stress

Failure rates for the normal full-power-operation reference case were calculated for steady-state operating conditions assuming no significant thermal gradient through the wall of the reactor pressure vessel. A study was conducted to determine the sensitivity of the calculated failure rates to possible thermal stresses. In Figure 5.16, the failure rate vs upper-shelf energy at a neutron-fluence level corresponding to EOL operation is presented for the normal full-power-operation reference variable condition, assuming both a zero thermal stress and a positive thermal stress at the inside diameter. The positive thermal stress is equal to the thermal stress calculated for normal reactor shutdown in the transition-temperature region. The results in Figure 5.16 indicate that assuming a positive thermal stress equal to that associated with normal shutdown operation can result in nearly an order of magnitude increase in calculated failure rate compared to full-power operating conditions where thermal stress is assumed to be equal to zero.

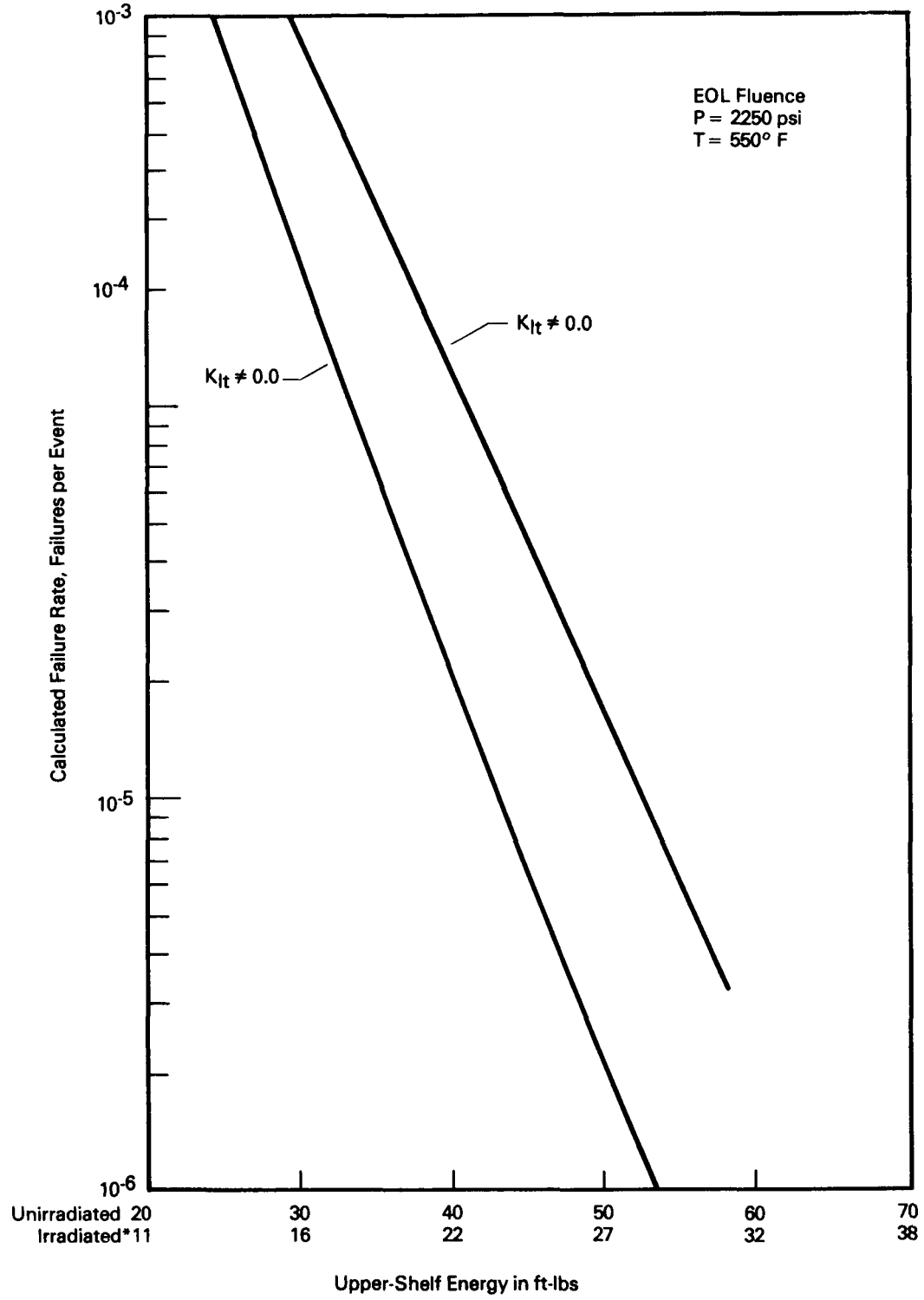

Figure 5.16: Thermal-Stress Sensitivity Study for Full-Power Operation at EOL Fluence

5.3 Anticipated Low-Temperature/Pressure Transients

During the period from 1969 to 1976, approximately 30 low-temperature/pressure excursions that exceeded the allowable pressure/temperature limits for normal startup and shutdown operations at operating domestic PWRs were reported (Ref. 9). The simulation program, which has the capability to simulate variable pressure and temperature or hold them at a specified constant value, was used to calculate the failure probability associated with these events for the generic PWR beltline region. The results of the low-temperature transient analysis generated with the simulation program are presented in Section 5.3.1. Section 5.3.2 presents sensitivity studies. Appendix A shows a comparison of the simulated results with those previously generated using the OCTAVIA code.

5.3.1 Reference Variable Condition

The low-temperature/pressure transients were evaluated using the simulation program. Pressure and temperature were treated as random variables to calculate the failure rate for reactor pressure vessels subject to the observed transients. Using the observed events described in Reference 9 and statistical-significance tests, it was determined that the pressure and temperature distributions could be represented by the Johnson S_B distribution (Ref. 11). Failure rates calculated using the simulation program were multiplied by a factor of 0.08, which corresponds to the observed frequency of events per year of reactor operation, as described in the OCTAVIA code.

The failure rates for a reactor pressure vessel subject to the observed overpressure events are presented in Table 5.1 for neutron-fluence levels corresponding to 2.25 EFPY, 10.0 EFPY, and EOL. The results indicate that without implementation of additional protective measures, the failure rate as a result of the inadvertent transients would increase by a factor of about 50 at the end of EOL fluence, compared to 2.25 EPFY.

Table 5.1: Calculated Failure Rates for Low-Temperature/ Pressure Transients

Fluence (EFPY)	Failure Rate (failures per reactor year)
2.25	9.5×10^{-6}
10.0	1.1×10^{-4}
EOL	5.3×10^{-4}

5.3.2 Anticipated Low-Temperature/Pressure-Transient Sensitivity Studies

5.3.2.1 Flaw Distribution

As in the previous sensitivity studies, the OCTAVIA EOL and Marshall preservice flaw distributions are used to define the sensitivity of calculated failure rate to a wide range of assumed flaw distributions, which could reasonably be expected to exist in a vessel at some point in its operating life. These calculated failure rates, adjusted to a per year basis, are presented in Table 5.2. The results in Table 5.2 indicate that the calculated failure rates are relatively insensitive to the assumed flaw distribution.

Table 5.2: Calculated Failure Rates as a Function of Flaw Distribution and Neutron Fluence for Low-Temperature/Pressure Transients

	Failure Rate (failures per reactor year)	
Fluence (EFPY)	OCTAVIA EOL Distribution	Marshall Preservice Distribution
2.25	9.5×10^{-6}	3.5×10^{-6}
10.0	1.1×10^{-4}	4.4×10^{-5}
EOL	5.3×10^{-4}	2.4×10^{-4}

5.3.2.2 Minimum Detectable Flaw Size

Sensitivity studies were conducted to determine the effect of minimum detectable flaw size on the calculated failure rate. Failure rates were calculated assuming that 0.125-in., 0.25-in., and 0.5-in. flaws, respectively, almost always are present and undetected in the vessel beltline. At neutron-fluence levels corresponding to 10 EFPY and EOL, the calculated failure rates were relatively insensitive to undetected flaw sizes up to 0.25 in. For an undetected flaw size of 0.5 in., the calculated failure rates increased approximately by an order of magnitude at both fluence levels.

5.4 Postulated High-Temperature/Pressure Transients

Failure rates were calculated for the typical reactor pressure vessel subjected to postulated high-temperature/pressure transients at neutron-fluence levels corresponding to 10 EFPY and EOL. These transients were assumed to occur at 550°F and to range from 3000 psi to 5000 psi. The vessel was assumed to have an initial, unirradiated upper-shelf energy of 65.0 ft-lbs; thermal stresses were assumed to be equal to zero.

5.4.1 Reference Variable Condition

Figure 5.17 presents the calculated failure rates vs pressure at neutron-fluence levels corresponding to 10 EFPY and EOL for the reference variable condition. The calculated failure rates range from approximately 10^{-3} to 10^{-5} failures per event, depending on the magnitude of the pressure transient and the neutron-fluence level. These results do not include the probability that the high-pressure transient will, in fact, occur.

5.4.2 Sensitivity Studies

5.4.2.1 Flaw Distribution

A study was conducted to determine the sensitivity of the calculated failure rate to the assumed flaw distribution for postulated high-temperature/pressure transients. Figures 5.18 and 5.19 present the calculated failure rates vs

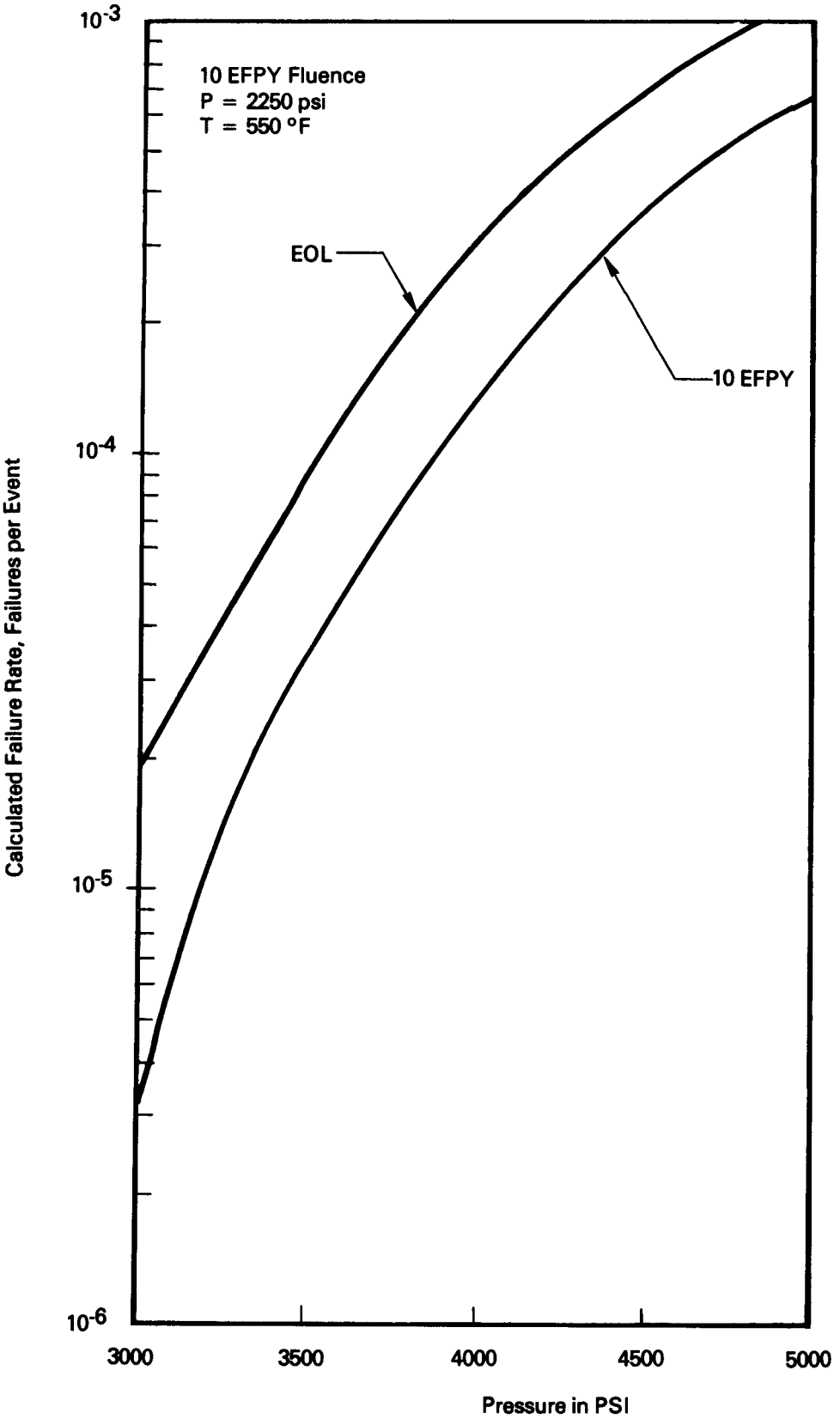

Figure 5.17: Failure Rate vs Pressure for Postulated High-Temperature/ Pressure Transients, Reference Variable Condition

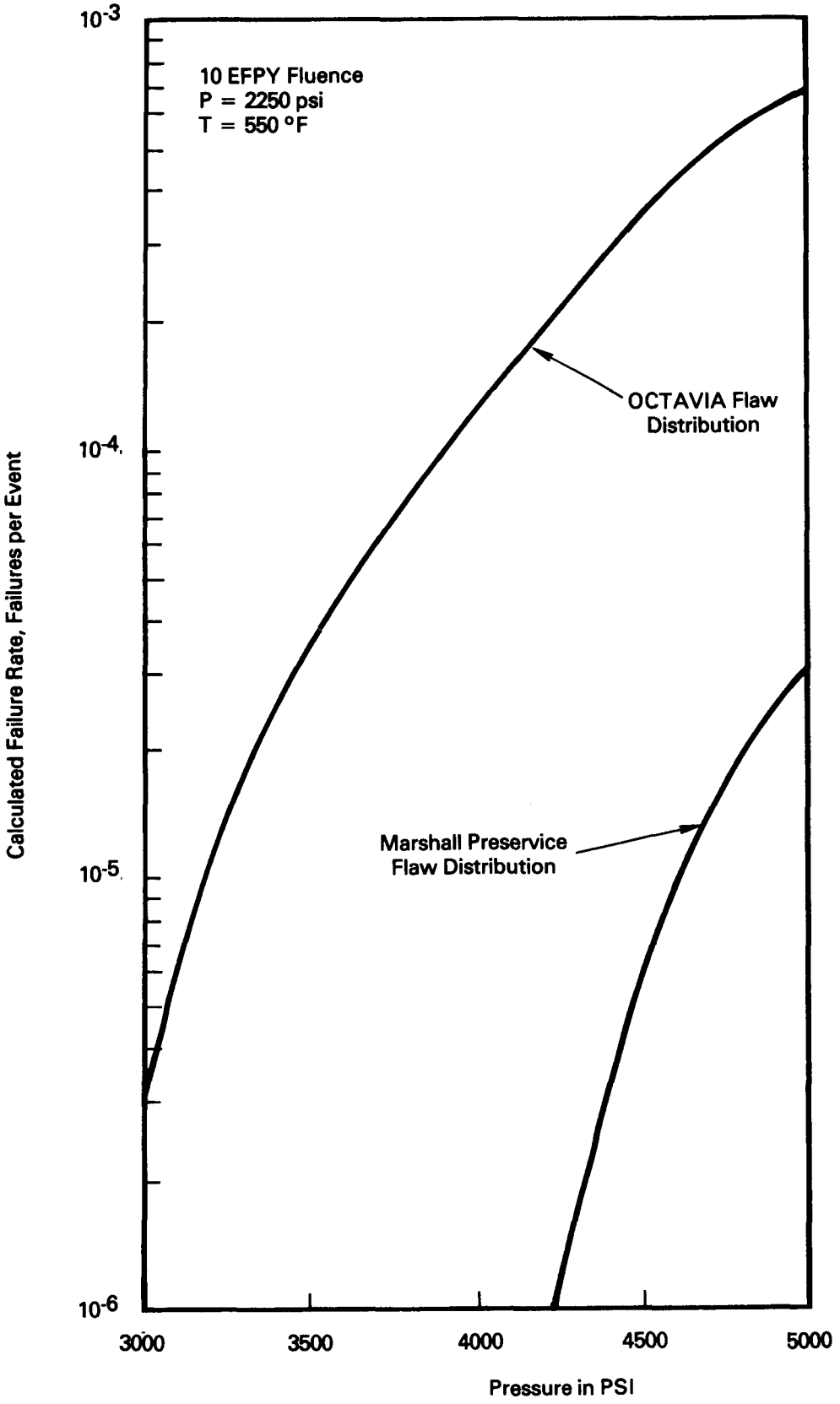

Figure 5.18: Flaw Distribution Sensitivity Study for Postulated High Temperature Pressure Transients at 10 EFPY Fluence.

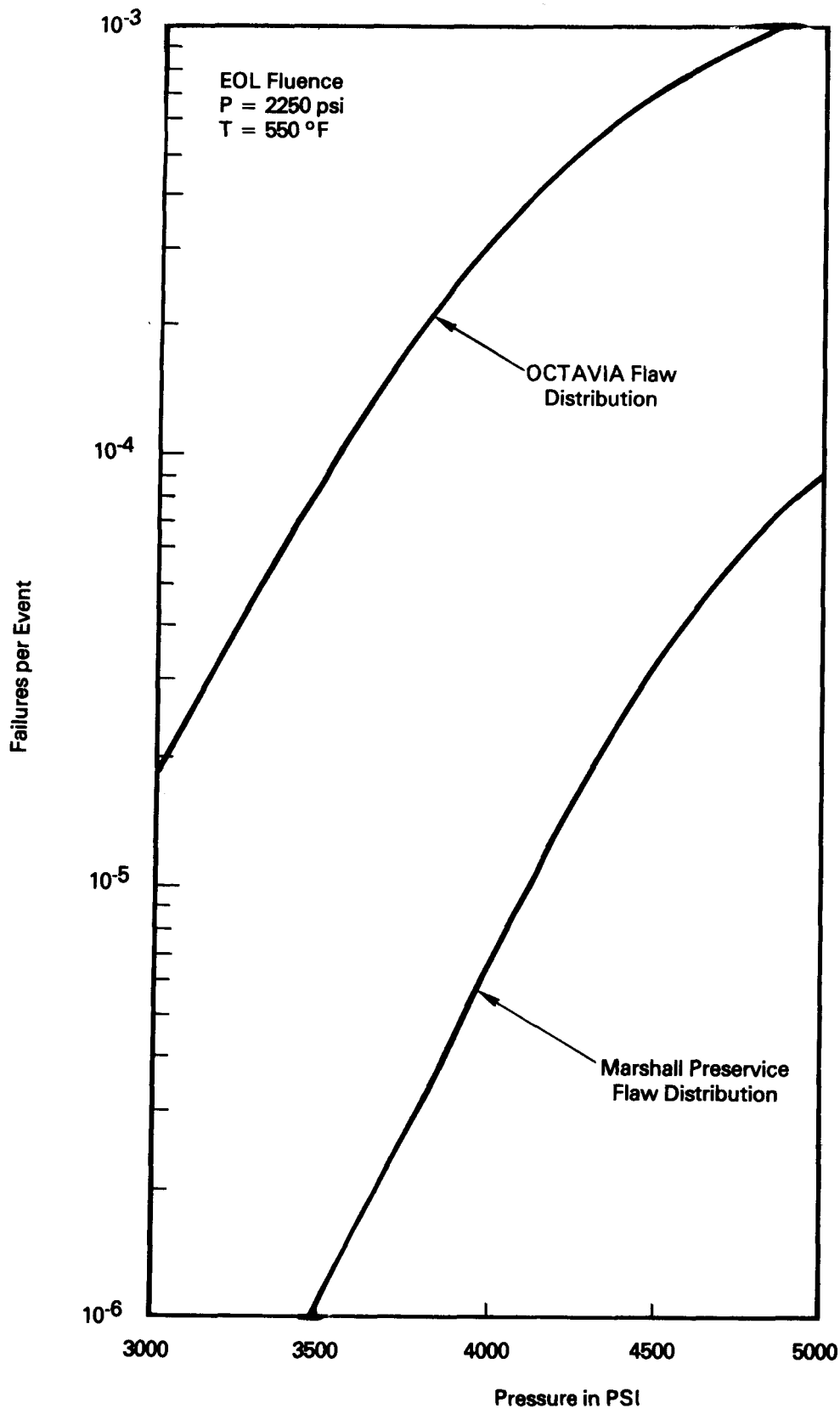

Figure 5.19: Flaw Distribution Sensitivity Study for Postulated High Temperature Pressure/Transients at EOL Fluence

pressure, for both Marshall preservice flaw distribution and the OCTAVIA distribution at neutron-fluence levels corresponding to 10 EFPY and EOL, respectively. Over the range of pressures considered, the failure rates determined from the Marshall preservice flaw distribution vary between one to two orders of magnitude less than the failure probabilities calculated for the OCTAVIA flaw distribution at each of the fluence levels.

5.4.2.2 Minimum Detectable Flaw Size

Sensitivity studies were conducted to determine the effect of minimum detectable flaw size on the calculated failure rate. Failure probabilities were calculated at pressures of 3000 psi and 5000 psi, assuming that 0.125-in., 0.25-in., 1.0-in., and 1.5-in. flaws, respectively, are almost always present and undetected in the vessel beltline.

At a neutron-fluence level corresponding to 10 EFPY, the calculated failure rate at 3000 psi pressure is relatively insensitive to undetected flaw sizes up to 1.5 in. For an undetected flaw size of 2.0 in., the failure probability increased approximately two orders of magnitude. At a neutron-fluence level corresponding to EOL, the calculated failure rate at 3000 psi is relatively insensitive to undetected flaw sizes up to 1.0 in. For an undetected flaw size of 1.5 in., the calculated failure rate increased by more than an order of magnitude. At both 10 EFPY and EOL fluence levels, the calculated failure rate for 5000 psi pressure was relatively insensitive to undetected flaw sizes up to 0.5 in. For an undetected flaw size of 1.0 in., the calculated failure rate increased nearly two orders of magnitude.

6 FURTHER DISCUSSION, SUMMARY, AND CONCLUSIONS

This study had three major objectives: (1) to better define the effect of neutron irradiation, material variation, and flaw distribution on the failure rate for the beltline region of PWR pressure vessels; (2) to estimate the relative margins against failure for normal operation and certain transient conditions associated with nuclear pressure vessels; and (3) to evaluate the current limitations for using fracture mechanics models to predict failure rates for nuclear pressure vessels. Several observations relative to these goals can be made from the results presented in Section 5.0.

First, copper content and flaw distribution have been shown to have a major influence on calculated failure rate. However, the degree of influence of these variables changes significantly depending on neutron fluence level and the pressure/temperature states associated with various reactor conditions.

The calculated failure rate is very sensitive to copper content where combinations of copper content, neutron fluence, and temperature result in reactor operation near the middle of the transition temperature region. In this region, relatively small variations in copper content produce relatively large changes in fracture resistance and significantly influence failure rate. In contrast, the failure rate is relatively insensitive to copper content where combinations of copper content, neutron fluence, and temperature result in reactor operation in or near either the lower- or upper-shelf temperature regions. In both these regions, the failure rate is relatively insensitive to copper content because wide variation in copper content does not produce large changes in fracture resistance.

For the range of variables included in this study, the failure rates associated with operating events that take place in the transition temperature region are very sensitive to medium and high levels of copper content at the 10 EFPY fluence level; the failure rate is somewhat less sensitive at lower copper levels where the variable conditions correspond to operation in the upper transition temperature region, near the upper shelf. At the EOL fluence level, the failure rate for events that occur in the transition temperature region is very sensitive to low and medium levels of copper content; the

failure rate is not sensitive to copper content at the higher levels of copper where the variable conditions correspond to operation in the lower-shelf temperature region. In the upper-shelf temperature region, the calculated results indicate that failure rate is only mildly sensitive to copper content over a wide range of neutron fluence. In contrast to the general trends indicated for copper content, the calculated failure rate is very sensitive to flaw distribution in the upper-shelf temperature region but is only mildly sensitive to flaw distribution in the transition temperature region.

The sensitivity of calculated failure rate to flaw distribution and copper content and results from sensitivity studies for other variables provide information from which conclusions can be drawn concerning margins against failure and the limitations of using fracture mechanics models to predict failure rate.

As Figures 5.1 and 5.2 indicate, the safety margins provided by the pressure/temperature limits specified by the ASME Code for reactor start-up and shutdown correspond to failure rates of approximately 10^{-7} failures per vessel year. The results presented in Figures 5.1 and 5.2 do suggest, however, that inaccuracies in reported copper content are important and that caution should be exercised when developing deterministic operational limits; that is, pressure/temperature limits constructed for vessels fabricated using procedures typically resulting in high and variable copper contents in welds should not be based on single reported copper contents that are relatively low.

The accuracy of the calculated failure rates indicated in Figures 5-1 and 5-2 should not be significantly affected by inaccuracies in the random variables. This is believed to be true because the failure rates are derived from variables that are either well defined or that produce relatively small changes in failure rate over range considered in this study. Specifically, the failure rate in the transition temperature region is only mildly sensitive to flaw distribution and the range of K_{IC}, the two variables having significant uncertainty. Although the failure rate is very sensitive to copper content at lower fluence levels, the copper content is relatively well defined for various classes of vessels.

For the upper-shelf temperature region, the results shown in Figure 5-10 indicate that the requirements for minimum unirradiated and irradiated upper-shelf energies of 75 and 50 ft-lb, respectively, correspond to failure rates less than 10^{-6} failures per vessel year. However, the results in Figure 5.12 also indicate that the sensitivity of failure rate to flaw distribution is significant. Consequently, because flaw distribution is a variable with significant uncertainty, the accuracy of the calculated failure rates in the upper-shelf temperature region cannot be well defined. Qualitatively, however, the calculated results imply that the minimum upper-shelf energy requirements provide adequate safety margins because, although the results are sensitive to flaw distribution, the range of flaw distribution used in the sensitivity studies is intuitively reasonable and the results are relatively insensitive to undetected flaw depths of up to 1 in.

Implicit in all the results presented in this study are the radiation damage model described in Reference 15, linear elastic fracture mechanics models for predicting vessel failure, and an assumption that the weld metal is the dominant failure contributor in the beltline region. The accuracy of each of these assumptions, while not considered explicitly in this study, will have an effect on the calculated results and their application; therefore, some additional comments about these assumptions are appropriate.

The damage model in Reference 15 is based on the test results obtained from specimens that had been irradiated in reactor surveillance capsules and test reactors. A review of the data obtained from reactor surveillance capsules indicates that the relationship between neutron fluence and shift in RT_{NDT} defined in Reference 15 for weld metal represents, within 5 or 10°F, an average line for the population of weld data for fluence levels up to 10^{19} n/cm^2. In the upper-shelf temperature region and at fluence levels about 10^{19} n/cm^2 in the transition temperature region, few surveillance data are available to make an accurate assessment of the damage model in these regions. Further, there are some very limited data that suggest that Reference 15 may overpredict irradiation damage at fluence levels in excess of 10^{19} n/cm^2 in both the transition and upper-shelf temperature regions. To determine what effect an overprediction at high fluence rates would have on failure rate, the failure rate in the upper-shelf temperature region was recalculated for the

EOL fluence level using the assumption that at fluences greater than 10^{19} n/cm^2 the reduction in upper-shelf energy was constant and equal to the reduction predicted at 10^{19} n/cm^2 by Reference 15. The resultant failure rate was determined to be within a factor of approximately two; this result indicates that the failure rate is essentially insensitive to the assumed damage saturation at high fluence levels. Based on the review of the data in the transition temperature region and the insensitivity to damage in the upper-shelf region, it is concluded that the damage model in Reference 15 does not introduce any significant inaccuracy into the failure rate calculations.

Linear elastic fracture mechanics is an accepted method to predict failure when conditions are such that initial crack extension results in unstable fracture from cleavage. For the stress conditions evaluated in this study, linear elastic fracture mechanics models should result in accurate failure estimates through most of the transition temperature. Recent work (Reference 19) in elastic plastic fracture mechanics has provided fracture models that generally are more appropriate for application in the upper-shelf temperature region; however, these methods and the materials data needed to apply the methods have not yet had wide application. Although the failure criterion employed in this study is not likely to predict nonconservative failure rates, an explicit determination of the accuracy of the results for the upper-shelf region cannot be defined until these newer methods and associated data can be applied.

The flaw distributions used in this study are estimates based on the volume of weld in the beltline region. The weld volume was used based on the belief that the weld metal is more likely than the base metal to contain crack-like defects and on the observation from reactor surveillance data that weld metal having high and variable copper content is more sensitive to neutron irradiation than is base metal with similar copper content. However, because the base metal in the beltline region can have 20 to 25 times more volume than the weld metal, it is difficult to determine what influence the base metal has without an estimate of how much less likely it is that the base metal will contain flaws compared to the weld metal. Consequently, some degree of uncertainty must be associated with the calculated failure rates. However,

the error associated with the effective beltline volume is likely to be small, especially for vessels having beltline welds with high and variable copper contents.

Based on the sensitivity studies and on consideration of the damage and failure models and the flaw distribution, it appears that the calculated failure rates are likely to be accurate within an order of magnitude for operational events that take place in the transition temperature region and within somewhat less than two orders of magnitude for operational events that take place in the upper-shelf temperature region. While this range of uncertainty may dictate limited use in applying the calculated failure rates in an absolute sense, the results can better be used to rank and discriminate between various failure contributors and to complement deterministic solutions for decision making purposes. The following examples illustrate applications in these areas.

Because the total probability of vessel failure is approximately equal to the sum of the failure probabilities associated with individual events, the calculated failure rates can be used to rank individual events according to the relative contribution to total failure rate and to identify conditions that may lead to unacceptable contributions to risk. For example, consider the failure rates associated with normal full-power operation, postulated high temperature/ pressure transients, and anticipated low temperature/pressure transients relative to a failure rate for the normal startup/shutdown sequence of approximately 10^{-7} failures per vessel year. The results given in Section 5.2.1 indicate that full-power operation in the upper-shelf temperature region at EOL fluence will provide the same relative failure rate as normal startup/shutdown if the initial, unirradiated upper-shelf energy is approximately 60 ft-lb. Similarly, as Figure 5.19 shows, a high temperature/ pressure transient at 4000 psi would have the same relative failure rate as normal startup/ shutdown at EOL fluence if the probability that the transient would occur was no greater than 10^{-3} events per vessel year. Based on this ranking, some action to reduce failure rate might be implemented for vessels having less than 60 ft-lb initial upper-shelf energy or for conditions that may result in high temperature pressure transients of 4000 psi that occur at a frequency greater than 10^{-3} events per vessel year.

Section 5.3 indicates that at EOL fluence the anticipated low temperature/pressure transients would result in relative failure rates that are two orders of magnitude higher than that associated with normal startup/shutdown operation if the transients were allowed to occur at the rate observed prior to 1978. This increased relative failure rate led, in part, to the installation of protective devices to decrease the transient frequency.

Finally, a comment concerning the relationship between failure rate and deterministic safety factors: several sensitivity studies in this report have indicated that for some operating conditions, the failure rate is only mildly sensitive or relatively insensitive to significant changes in variables, such as flaw distribution and K_{IC}. These variables typically are used with safety factors or as bounding values to establish deterministic operating limitations. In such cases, caution must be exercised in attaching significance to these variables when setting operating limits. For example, failure rate is insensitive to the range of K_{IC} when K_{IC} is allowed to vary beyond the range $K_{IC} \pm 2\sigma$. However, different deterministic operating limits and associated levels of reliability would be obtained by using 2, 3, or 4 sigma limits for K_{IC}. In this instance, the actual levels of reliability could not be accurately assessed from the K_{IC} range alone because it has no effect on failure rate. The level of reliability associated with the different deterministically determined operating limits could only be evaluated by determining the relative failure rates for the entire system depicted in Figure 2.1 at each of the distinct operating limits. The failure rate calculation using the entire system interaction provides a necessary complement for the application of safety factors to single-valued variables, for setting deterministic limits on operating conditions, and for evaluating the relative levels of reliability associated with the variable values and operating limits.

The work in this study focused on normal operating and transient conditions where the thermal stresses are relatively small compared to pressure stress. However, there is an important class of transients where thermal stresses are significant. To estimate the total failure rate for the beltline region of PWRs, additional work is required to define the relative contribution to failure rate from this class of transient events.

7 REFERENCES

Documents marked with an asterisk are available for purchase from the National Technical Information Service (NTIS), Springfield, Virginia 22161. Documents marked with two asterisks are available from NTIS and from the NRC/GPO Sales Program, USNRC, Washington, D.C. 20555. Other documents are available at the address given in their citation or at public technical libraries.

(1) C. A. G. Phillips and Warwick, "A Survey of Defects in Pressure Vessels Built to High Standards of Construction and Its Relevance to Nuclear Primary Circuit Envelopes," UKAEA Report, AHSB(S)R 162, 1967.

(2) O. Kellermann and H. G. Seipel, "Analysis of the Improvement in Safety Obtained by a Containment and by Other Safety Devices for Water Cooled Reactors," IAEA Symposium on the Containment and Siting of Nuclear Power Plants, Vienna, April 1967.

(3) Advisory Committee on Reactor Safeguards, "Report on the Integrity of Reactor Vessels for Light-Water Power Reactors," U.S. Atomic Energy Commission, WASH-1285, 1974.*

(4) U.S. Atomic Energy Commission Regulatory Staff, "Technical Report on Analysis of Pressure Vessel Statisitics from Fossil-Fueled Power Plant Service and Assessment of Reactor Vessel Reliability in Nuclear Power Plant Service," U.S. Atomic Energy Commission, WASH-1318, 1974.*

(5) American Society of Mechanical Engineers (ASME), Boiler and Pressure Vessel Code, The American Society of Mechanical Engineers.

(6) P. E. Becker and A. Pedersen, "Application of Statistical Linear Elastic Fracture Mechanics to Pressure Vessel Reliability Analysis," International Conference on Structural Mechanics in Reactor Technology, Berlin, September 1973.

(7) Study Group Report, "An Assessment of the Intensity of PWR Pressure Vessels," UKAEA Report, October 1976.

(8) G. Zech, "Reactor Vessel Pressure Transient Protection for Pressurized Water Reactors," U.S. Nuclear Regulatory Commission Report NUREG-0224, 1978.**

(9) W. E. Vesely, E. K. Lynn, and F. F. Goldberg, "The OCTAVIA Computer Code: PWR Reactor Pressure Vessel Failure Probabilities Due to Operationally Caused Pressure Transients," U.S. Nuclear Regulatory Commission Report, NUREG-0258, 1978.**

(10) ASME, Boiler and Pressure Vessel Code, Section III, Appendix G, The American Society of Mechanical Engineers.

(11) Code of Federal Regulations, Title 10, Part 50, Appendix G, Office of the Federal Register, U.S. Government Printing Office, 1980.*

(12) G. J. Hahn and S. S. Shapiro, Statistical Models in Engineering, John Wiley and Sons, Inc., 1967.

(13) R. E. Shannon, Systems Simulation: The Art and Science, Prentice-Hall, Inc., 1975.

(14) ASME, Boiler and Pressure Vessel Code, Section III, Paragraph NB-2331, The American Society of Mechanical Engineers.

(15) U.S. Nuclear Regulatory Commission, Regulatory Guide 1.99, "Effects of Residual Elements in Predicted Radiation Damage to Reactor Vessel Materials," Revision 1, U.S. Nuclear Regulatory Commission, April 1977.**

(16) Shabbits and others, "Heavy Section Fracture Toughness Properties of A533 Grade B Class 1 Steel Plate and Submerged Arc Weldment," WCAP-7414, Westinghouse Electric Corporation, Pittsburgh, December 1969.

(17) American Society for Testing and Materials, "Standard Method of Test for Plane-Strain Fracture Toughness of Metallic Materials," E399-74, Annual Book of ASTM Standards.

(18) J. M. Barsom and S. T. Rolfe, "Correlations Between K_{IC} and Charpy V-Notch Test Results in the Transition-Temperature Range," ASTM, STP 466, March 1970.

(19) P. C. Paris and others, "A Treatment of the Subject of Tearing Instability," U.S. Nuclear Regulatory Commission Report NUREG-0311, August 1977.**

APPENDIX A

COMPARISON OF CALCULATED FAILURE RATE FOR ANTICIPATED LOW-TEMPERATURE/PRESSURE TRANSIENTS USING THE SIMULATION AND OCTAVIA PROGRAMS

In early 1978, the Office of Nuclear Regulatory Research, U.S. Nuclear Regulatory Commission, developed the OCTAVIA computer code (as described in Ref. 9 of the main body of this report) to calculate the probability of reactor-pressure-vessel failure as a result of low-temperature/pressure transients. A study was conducted to compare results obtained using the OCTAVIA code and the simulation program.

In the comparison study, the simulation program first was made to correspond as closely as possible to the OCTAVIA code. This provided a check on the calculational procedures used in the simulation program. Pressure and flaw size were simulated, but temperature, copper content, and initial RT_{NDT} were held constant at 134°F, 0.25% and 9°F, respectively. Although the simulation code has the capability of treating temperature, copper content, and initial RT_{NDT} as random variables, the OCTAVIA code is limited to evaluating constant values for these variables. The 134°F temperature corresponds to the mean value of the temperature distribution of the observed low-temperature/pressure transients. The flaw distribution used corresponded to that in the OCTAVIA code, and the mean fracture-toughness value was calculated from the fracture-toughness-vs-adjusted-temperature curve used in the OCTAVIA code. (Other failure probabilities discussed in this report are based on the updated fracture-toughness-vs-temperature relation shown in Figure 4.3, which incorporated additional data.)

Table 1 presents for comparison the failure probabilities calculated by the simulation program and the median failure probabilities predicted by the OCTAVIA code at neutron-fluence levels corresponding to 2.25 EFPY, 10 EFPY, and EOL.

Table 1: Simulated and OCTAVIA Failure Rates for Low-Temperature/ Pressure Transients with Constant Copper Content, Initial RT_{NDT}, and Temperature*

Fluence (EFPY)	Failure Rate (failures per reactor year) Simulation Code	OCTAVIA	Ratio of Simulated Failure Rate to OCTAVIA Failure Rate
2.25	1.6×10^{-7}	4.8×10^{-7}	0.30
10.0	6.9×10^{-5}	6.6×10^{-5}	1.05
EOL	1.7×10^{-4}	1.2×10^{-4}	1.42

*Constant 134°F temperature, 0.25% copper content and 9.0°F initial RT_{NDT}; K_{IC} vs $(T-RT_{NDT})$ curve from the OCTAVIA code

The last column in the table presents the ratios of the simulated failure probabilities. At a neutron-fluence level corresponding to 2.25 EFPY, the OCTAVIA program predicts a failure rate approximately 3 times greater than that predicted by the simulation program. At neutron-fluence levels corresponding to 10 EFPY and EOL, the predicted failure rates are within a factor of 1.5. Thus there is good correlation between the results derived by the two techniques.

A comparison also can be made of the effect of simulating certain variables as opposed to holding them constant (as is the case in the OCTAVIA code). Table 2 summarizes the results from the simulation code first when copper, initial RT_{NDT}, pressure, temperature, and flaw size are used as random variables and second

Table 2: Comparison of Failure Rates Calculated by Simulating or Holding Constant the Variables Copper Content, Initial RT_{NDT}, and Temperature for Low-Temperature/Pressure Transients

Fluence (EFPY)	Failure Rate (failures per reactor year)	
Fluence (EFPY)	Simulated Variables	Constant Variables
2.25	9.5×10^{-6}	4.2×10^{-7}
10.0	1.1×10^{-4}	7.7×10^{-5}
EOL	5.3×10^{-4}	4.0×10^{-4}

when only pressure and flaw size are used as random variables, as is the case in the OCTAVIA code. The updated fracture toughness curve shown in Figure 4.3 was used to perform the calculations in Table 2.

At the three fluence levels the failure rates are greater when copper content, RT_{NDT}, and temperature are simulated than when they are held constant, as in the OCTAVIA code. The largest difference in failure probabilities is at the lowest fluence level, where the simulated failure rate is approximately a factor of 20 greater than that predicted by the OCTAVIA code. At the higher fluences, simulating temperature, copper content, and initial RT_{NDT} has a smaller effect because the fracture-toughness-vs-temperature curve is relatively flat. Consequently, K_{IC} is relatively insensitive to changes in temperature, copper content, and intial RT_{NDT}, and the failure rates tend to become coincident.

APPENDIX B

IMPROVED MONTE CARLO SIMULATION OF RARE EVENT FAILURES

DOROTHY S. NG
RONALD W. WOLFF
ROBERT T. LANGLAND

LAWRENCE LIVERMORE LABORATORY
UNIVERSITY OF CALIFORNIA
LIVERMORE, CALIFORNIA

PREPARED FOR NUCLEAR REGULATORY COMMISSION

DESCRIPTION OF THE SIMULATION THEORY

Introduction

Because of the interest in failure rates in the range of 10^{-6}, an importance-sampling scheme was developed to increase the efficiency of the simulation routine depicted in Figure 3.1 of the main body of this report. The importance-sampling procedure was used primarily to generate the constant 10^{-7} failure-rate paths in the transition-temperature region to provide a check on the accuracy of simulated results. The results described in this appendix are applicable only for flaws that extend into the vessel wall from the inside surface.

Probability of Failure Calculation

The failure of a pressure vessel is modeled in terms of the applied stress intensity factor, K_I, and the allowable stress intensity factor, K_{IC}. The vessel will fail if it contains a crack such that at the location of the crack,

$$K_I \geq K_{IC} \tag{1}$$

Both of these quantities depend on many parameters which are known for a particular vessel. Four of these quantities are treated as random variables. The random quantities are

- Z: Crack depth a discrete random variable with nine possible values. Let $P(Z_i = z_i) = \alpha_i$, $i = 1, 2, \ldots 9$
- Cu: % copper, distributed as a truncated normal
- RTI: Initial RT_{NDT}, distributed as a normal
- R: Distributed as a truncated normal N(0,1)

In the simulation, the applied stress intensity K_I is a function of many variables but generally only one random variable, crack depth. For a selected crack depth, K_I can be calculated. The allowable stress intensity is a

function of the three random variables, Z (the crack depth), Cu (the percent of copper), and RTI (the inital value of RT_{NDT}), and R (a normal distribution of K_{IC}). The failure simulation sample values of Z, Cu, RTI. The sampled values are used to calculate the K_I and the mean value of K_{IC}. Finally the value of K_{IC}, the allowable stress intensity factor, is determined by sampling from a truncated normal distribution to obtain the value of R. K_{IC} is calculated from the expression below, where μ is the mean value for K_{IC}.

$$K_{IC} = (RS+1)\mu \tag{2}$$

S = 0.1074498. This process is repeated, and failures are counted every time $K_I > K_{IC}$. For example, if 10 failures occur in 1,000,000 trails, then the estimate of the probability of failure is $10 \div 1{,}000{,}000 = 10^{-5}$.

The final value of K_{IC} is obtained by sampling from a truncated normal distribution given the mean value of K_{IC} (μ), which is a function of Z, Cu, and RTI. This suggested the probability of failure for a given trial, j, can be calculated as the conditional probability that $K_I > K_{IC}$, given the values of Z, Cu, and RTI, or

$$P = P(K_I \geq K_{IC}/Z, Cu, RTI) \tag{3}$$

$$P = P(R \geq (K_I - \mu)/\mu S/Z, Cu, RTI) \tag{4}$$

This conditional probability calculation on each trial, j, is the basis of the first improvement to the original simulation. For each trial, j, generate Z, Cu, RTI. Determine values for K_I and μ and call them K_{Ij} and μ_j, respectively. Calculate the quantity aj

$$aj = (K_{Ij} - \mu_j)/\mu_j \, S \tag{5}$$

Then the tail of the truncated normal distribution is integrated to yield

$$P_j = P(R \leq aj) \tag{6}$$

where

$$P_j = \int_{-3}^{aj} (1/\sqrt{2\pi}) e^{-\chi^2/2} dx \qquad (7)$$

The distribution is truncated at the 3σ limits. Correction for this truncation will only affect the results by 0.3% and is therefore ignored.

The final estimate of probability of failure is calculated by summing on the P_j's and dividing by the total number of simulations or trails.

$$\hat{P} = \left(\sum_{j=1}^{n} P_j \right) \div n. \qquad (8)$$

This estimator has a variance

$$V(\hat{P}) = V(P_j) \div n \qquad (9)$$

where

$$V(P_j) = \frac{\sum_{j=1}^{N} (P_j - \hat{P})^2}{n-1} \qquad (10)$$

The variance V(P) is a measure of the accuracy of the simulation and the estimator.

Elimination of Strata

Our physical understanding of the failure process indicates the probability of failure is much greater for larger crack depths. Preliminary runs of the original simulation revealed that failure does not occur for the shortest crack depth, $z_1 = 0.125$. It was decided to eliminate this stratum from the crack depth distribution used in the simulation. The probability $P(Z = z_1)$ was added to that for crack depth $Z_2 = 0.25$. In the notation $P(Z = z_1) = \alpha_i$

the probability of the crack depth, as altered in the original simulation, has $\alpha_1 = 0$, $\alpha_2 = .97132$, $\alpha_3 = .99632$, $\alpha_4 = .99882$, $\alpha_5 = .99962$, $\alpha_6 = .99987$, $\alpha_7 = .99995$, $\alpha_8 = .99998$, and $\alpha_9 = 1.00000$.

This alteration could potentially bias the simulation results by generating failure when $Z = z_2$ that would not have occurred. Fortunately, however, our calculations reveal that no harm was done since failure when the crack depth is $z_2 = 0.25$ is (virtually) impossible. That is, for practical purposes, $P_2 = 0$.

About 97% of the trials (100 α_2) have crack depth z_2; there is no need to perform these calculations. Thus, this stratum also should be eliminated from the crack depth distribution. However, it is not appropriate to add α_2 to α_3. Instead, we define a new conditional distribution of Z given $Z > z_2$

$$\gamma_i = P(Z = z_i \ / \ Z > z_2) = \alpha_i/(1-\alpha_2), \ i = 3, 4, \ldots, 9 \qquad (11)$$

and use this as the new distribution of crack depth in the simulation.

We now combine the direct integration of the probability of failure to obtain an estimate of $P(K_I \geq K_{IC} \ / \ Z > z_2)$. Since $P_2 = 0$, the failure probability is

$$\hat{P} = P(K_I \geq K_{IC} \ / \ Z > Z_2, \ Cu, \ RTI) \ (1 - \alpha_2) \qquad (12)$$

To estimate $\hat{P}$, use

$$\hat{P} = \left(\sum_{j=1}^{n} P_j \div n \right) (1 - \alpha_2) \qquad (13)$$

Our esimated improvement factor by eliminating Z_2 is

$$1/(1 - \alpha_2) \approx 35 \qquad (14)$$

To estimate the total improvement, this factor is multiplied by the improvement gained by direct integration of the conditional probability.

Inverse Sampling

We need to determine the run length for any given precision. To do this, we must estimate $\hat{P}$ and $V(P_j)$. A simple way to do this is known as the two-sample technique. For the initial run (sample), we estimate $\hat{P}$ and $V(P_j)$, treat the estimates as though they were the true values, and from them determine the run length. This technique would use equations (8), (9), and (10).

While the two-sample technique is simple in principle, choosing an initial n, say n_1, is difficult because P may vary widely from run to run, for example, from 10^{-3} to 10^{-6}. We may easily overshoot. n_1 may be greater than the value of n we need. On the other hand, if n_1 is too small, our esimates of $\hat{P}$ and $V(P_j)$ will be very inaccurate. Since the event $(P_i > 0)$ has low probability, the estimate of $V(P_j)$ is likely to be very poor if n_1 is too small.

A more reliable way to estimate the run length required for a given precision is to control the number, m, of positive P_j's, rather that the number of trials. The procedure to do this is a modification of what is known as inverse sampling.

Let $\pi = P(P_j > 0)$ and Q_k be the kth positive P_j, $k = 1, 2, \ldots, m$. Then the expected value of Q_k is

$$E(Q_k) = E(P_j \mid P_j > 0), \text{ and}$$

the probability of failure is

$$\hat{P} = E(Q_k)\pi \tag{15}$$

By inverse sampling, we choose m and let n be a random variable. Under this stopping rule, an unbiased estimator of π is

$$\hat{\pi} = (m - 1)/(n - 1) \tag{16}$$

where it can be shown that an (approximate) formula for the variance of $\hat{\pi}$ (good for small π and $m \geq 10$) is

$$V(\hat{\pi}) \simeq \pi^2/(m - 2) \tag{17}$$

Similarly, an unbiased estimator of $E(Q_k)$ is the sample mean of the m observed values

$$\bar{Q} = \sum_{k-1}^{m} Q_k/m \tag{18}$$

with variance

$$V(\bar{Q}) = V(Q_k)/m \tag{19}$$

To estimate P, we replace the quantities in equation (15) by their estimators equations (16) and (18). Our esimator of P is

$$\hat{P} = \bar{Q}\,\hat{\pi} = \frac{(m-1)\sum_{k=1}^{m} Q_k}{(n-1)m} \tag{20}$$

(Since n will usually be quite large, e.g., $n > 10^3$) we can replace (n-1) by n in (20)).

Because m is fixed, $\bar{Q}$ and $\hat{\pi}$ are independent random variables. Consequently, $E(\hat{P}) = P$ and an approximation for the variance is

$$V(\hat{P}) \simeq \hat{P}^2/(m-2) + \pi^2 V(Q_k)/m \tag{21}$$

To estimate (21), use

$$\hat{V}(\hat{P}) = \hat{P}^2/(m-2) + \hat{\pi}^2 \hat{V}(Q_k)/m \tag{22}$$

where

$$\hat{V}(Q_k) = \left(\sum_{k=1}^{m} Q_k^2 - m\,\bar{Q}^2\right) / (m-1) \tag{23}$$

The only question that remains is the choice of m. To obtain the same precision as the original simulation, 100 r% of the mean, choose m so that

$$V(\hat{P}) = (r\hat{P})^2 \tag{24}$$

If the second term on the right hand side of equation (21) were equal to zero, we would get $m = 1/4^2 + 2$. On the other hand, if $V(Q_k) = E^2(Q_k)$, the approximate value of $m = 2/r^2$. Trial runs have shown that $V(Q_k)/E^2(Q_k)$ varies widely from run to run but is nearly always greater than 1.

A two-sample technique for m is as follows: Choose an initial $m_1 = 2/r^2$. (Thus, if r = .1 (10%), choose $m_1 = 200$.) Estimate $\hat{\pi}$, $\hat{P}$, and $\hat{V}(Q_k)$ in equations (16), (20), and (23) with m replaced by m_1 and n replaced by n_1, where n_1 is the number of trials required to obtain m_1 positive P_j's. Use these estimates in the following equation and solve for m

$$\hat{P}^2/(m-2) + \hat{\pi}^2\, V(Q_k)/m = (r\hat{P})^2 \tag{25}$$

Resume the simulation until we get $(m - m_1)$ additional positive P_j's.

The quantities of equation (20) and the <u>square root</u> of equation (22) should be recomputed for the entire run and reported as the estimate of P, $\hat{P}$, and an estimate of its standard deviation. For r = .1, the estimated standard deviation should be (about) 10% of $\hat{P}$.

Relative to the original simulation, the efficiency factor of the direct integration of the probability is estimated as

$$\hat{P}/\hat{V}(P_j) = \sum_{k=1}^{m} Q_k \;/\; \sum_{k=1}^{m} Q_k^2 \tag{26}$$

The total improvement that includes stratification, is given as a product equations (14) and (26). This is expressed in the following equation

$$\text{Total efficiency} = \left(\frac{1}{1-\alpha_2} \right) \left(\frac{\sum_{k=1}^{m} Q_k}{\sum_{k=1}^{m} Q_k^2} \right) \qquad (27)$$